Chemical Geology 334 (2012) 324–344

Contents lists available at SciVerse ScienceDirect

Chemical Geology

journal homepage: www.elsevier.com/locate/chemgeo

Crustal versus source processes recorded in dykes from the Northeast volcanic rift zone of Tenerife, Canary Islands

F.M. Deegan [a,b,*], V.R. Troll [a,c], A.K. Barker [a], C. Harris [d], J.P. Chadwick [e], J.C. Carracedo [c], A. Delcamp [f]

[a] Department of Earth Sciences (CEMPEG), Uppsala University, 75236 Uppsala, Sweden
[b] Laboratory for Isotope Geology, Swedish Museum of Natural History, SE-104 05 Stockholm, Sweden
[c] Departamento de Física (GEOVOL), Universidad de Las Palmas de Gran Canaria, Las Palmas de Gran Canaria, Canary Islands, Spain
[d] Department of Geological Sciences, University of Cape Town, Rondebosch 7701, South Africa
[e] Science Gallery, Trinity College Dublin, Dublin 2, Ireland
[f] Department of Geography, Vrije Universiteit Brussels, Belgium

ARTICLE INFO

Article history:
Received 24 February 2012
Received in revised form 17 September 2012
Accepted 3 October 2012
Available online 12 October 2012

Editor: L. Reisberg

Keywords:
Tenerife
Ocean islands
Volcanic rift zones
O–Sr–Nd–Pb isotopes
Crustal contamination
Mantle sources

ABSTRACT

The Miocene–Pliocene Northeast Rift Zone (NERZ) on Tenerife is a well exposed example of a feeder system to a major ocean island volcanic rift. We present elemental and O–Sr–Nd–Pb isotope data for dykes of the NERZ with the aim of unravelling the petrological evolution of the rift and ultimately defining the mantle source contributions. Fractional crystallisation is found to be the principal control on major and trace element variability in the dykes. Differing degrees of low temperature alteration and assimilation of hydrothermally altered island edifice and pre-island siliciclastic sediment elevated the $\delta^{18}O$ and the $^{87}Sr/^{86}Sr$ ratio of many of the dykes, but had little to no discernible effect on Nd and Pb isotopes. Once the data are screened for alteration and shallow level contamination, the underlying source variations of the NERZ essentially reflect derivation from a young High-μ (HIMU, where $\mu = {}^{238}U/{}^{204}Pb$)-type mantle component mixed with depleted mid-ocean ridge-type mantle (DMM). The Pb isotope data of the NERZ rocks ($^{206}Pb/^{204}Pb$ and $^{207}Pb/^{204}Pb$ range from 19.591 to 19.838 and 15.603 to 15.635, respectively) support a model of initiation and growth of the rift from the Central Shield volcano (Roque del Conde), consistent with latest geochronology results. The similar isotope signature of the NERZ to both the Miocene Central Shield and the Pliocene Las Cañadas central volcano suggests that the central part of Tenerife Island was supplied from a mantle source that remained of similar composition through the Miocene to the Pliocene. This can be explained by the presence of a discrete column of young HIMU-like plume material, ≤100 km in vertical extent, occupying the melting zone beneath central Tenerife throughout this period. The most recent central magmatism on Tenerife appears to reflect greater entrainment of DMM material, perhaps due to waning of the HIMU-like "blob" with time.

1. Introduction

Ocean island rift zones are volcanic and intrusive alignments that play an important role in controlling island growth. They have been well studied in the Canary Islands, particularly with respect to their structural development (e.g. Carracedo, 1994, 1999; Walter and Schmincke, 2002; Walter and Troll, 2003; Walter et al., 2005; Carracedo et al., 2007, 2011; Delcamp et al., 2010, 2012). Canary Island rift zones are generally long-lived, dynamic structures, whose life spans are punctuated by giant collapse events (e.g. Carracedo, 1994; Watts and Masson, 1995; Carracedo et al., 2011). Flank collapses may, in turn, influence the petrologic evolution of rift zone magmas by disrupting the underlying plumbing system and promoting initially increased mafic volcanism that is later followed by magma differentiation at higher crustal levels (cf. Longpré et al., 2009; Manconi et al., 2009; Carracedo et al., 2011). Rift zones may therefore demonstrate a large degree of petrological variability, and the magma feeding them may undergo a variety of differentiation processes, including fractional crystallisation, magma-mixing, and crustal assimilation during storage within the island edifice (Clague et al., 1995; Klügel et al., 2000; Stroncik et al., 2009; Troll et al., 2012). When looking at the elemental and isotope chemistry of ocean island rift zone magmas, it is vital to first decipher and quantify these processes before evaluating the primary mantle signatures.

The isotopic compositions of ocean island magmas are frequently employed as probes of the mantle, and exhibit variations consistent with mixing of several isotopically extreme end-member components (Zindler and Hart, 1986). Included in these are: 1) depleted MORB mantle (DMM), characterised by high $^{143}Nd/^{144}Nd$ and the lowest Sr–

* Corresponding author at: Laboratory for Isotope Geology, Swedish Museum of Natural History, Box 50 007, SE-104 05 Stockholm, Sweden. Tel.: +46 18 51954074.
E-mail addresses: Frances.Deegan@geo.uu.se, Frances.Deegan@nrm.se (F.M. Deegan), Valentin.Troll@geo.uu.se (V.R. Troll), Abigail.Barker@geo.uu.se (A.K. Barker), Chris.Harris@uct.ac.za (C. Harris), jane.chadwick@sciencegallery.com (J.P. Chadwick), jcarracedo@proyinves.ulpgc.es (J.C. Carracedo), delcampa@tcd.ie (A. Delcamp).

0009-2541/$ – see front matter © 2012 Elsevier B.V. All rights reserved.
http://dx.doi.org/10.1016/j.chemgeo.2012.10.013

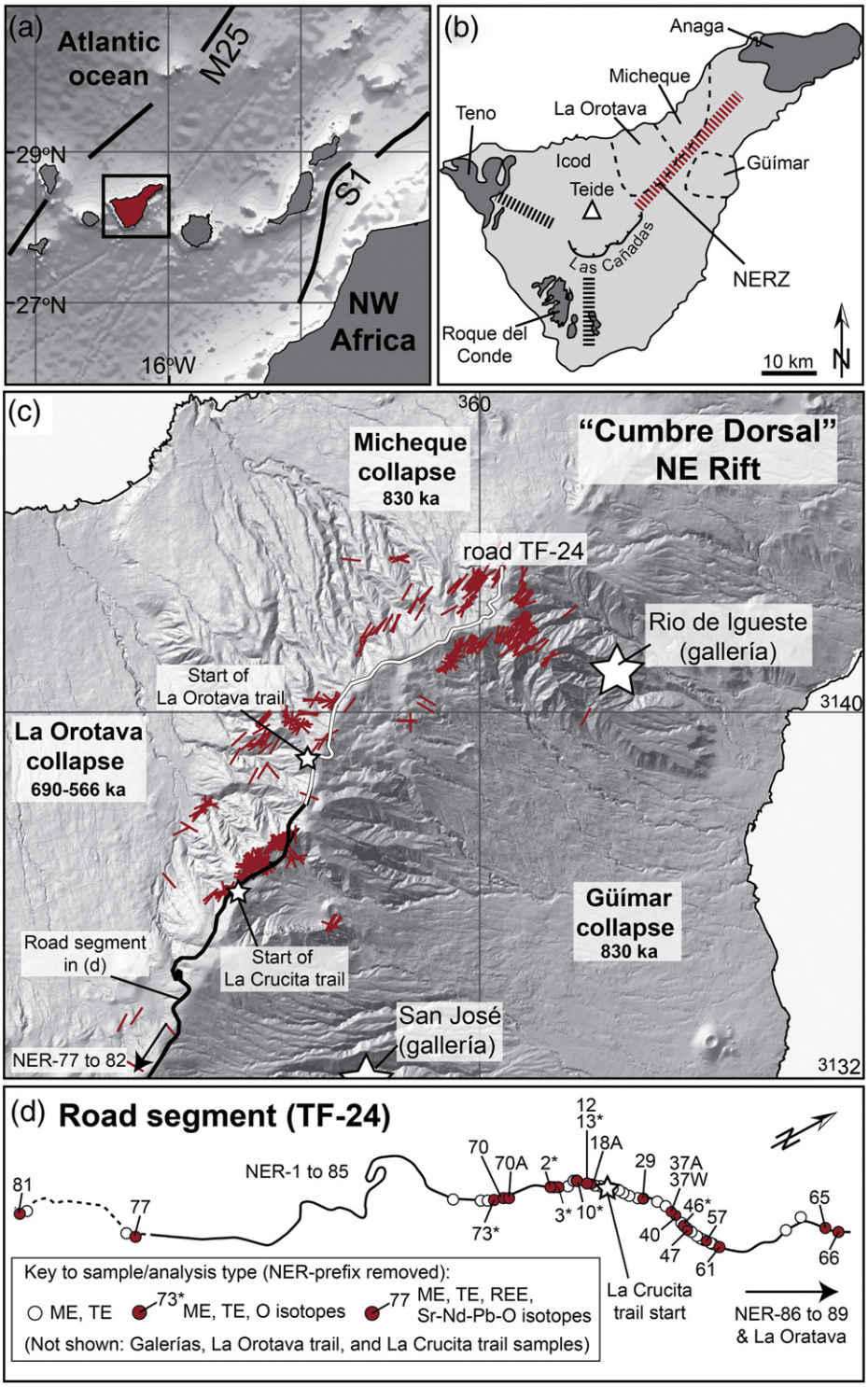

Fig. 1. a: Map of the Canary Archipelago, located off the coast of NW Africa between magnetic anomalies S1 (175 Ma) and M25 (156 Ma) (Roeser, 1982) with Tenerife highlighted. b: Simplified geological map of Tenerife showing i) the location of the shield basalt massifs Roque del Conde (the Central Shield), Teno, and Anaga, ii) the three rift zones (thick dashed black lines) and the collapse scars flanking the NERZ, iii) the Las Cañadas caldera wall, and iv) the location of the Teide volcanic complex at the junction of the rift zones and within the Icod landslide scar. c: Shaded relief map of the NERZ showing the distribution of dykes along the rift (short red lines) and the three collapse depressions flanking the ridge. The road TF-24 is shown, along which there is good exposure of the rift zone dykes. Most of the dykes analysed in this study were sampled along the segment of TF-24 highlighted in black and shown in detail in (d). The start of the trails "La Orotava" and "La Crucita" leading away from the main road, and the locations of the entrance to two gallerías are also shown. d: Detail of a segment of the road TF-24 along which most of the analysed dykes were sampled. Samples used for isotopic analysis from this road segment are highlighted in red and labelled. (For interpretation of the references to colour in this figure legend, the reader is referred to the web version of this article.)

Pb isotope ratios of all the mantle components, 2) enriched mantle (EM 1 and 2) with variable $^{87}Sr/^{86}Sr$, low $^{143}Nd/^{144}Nd$, and high $^{207}Pb/^{204}Pb$ and $^{208}Pb/^{204}Pb$ at a given $^{206}Pb/^{204}Pb$ and 3) high-μ (HIMU, where $\mu = {}^{238}U/^{204}Pb$) which has low $^{87}Sr/^{86}Sr$, intermediate $^{143}Nd/^{144}Nd$, the highest Pb ratios of the mantle components, and is thought to involve subducted ocean crust with long mantle residence times (see Hoffman,

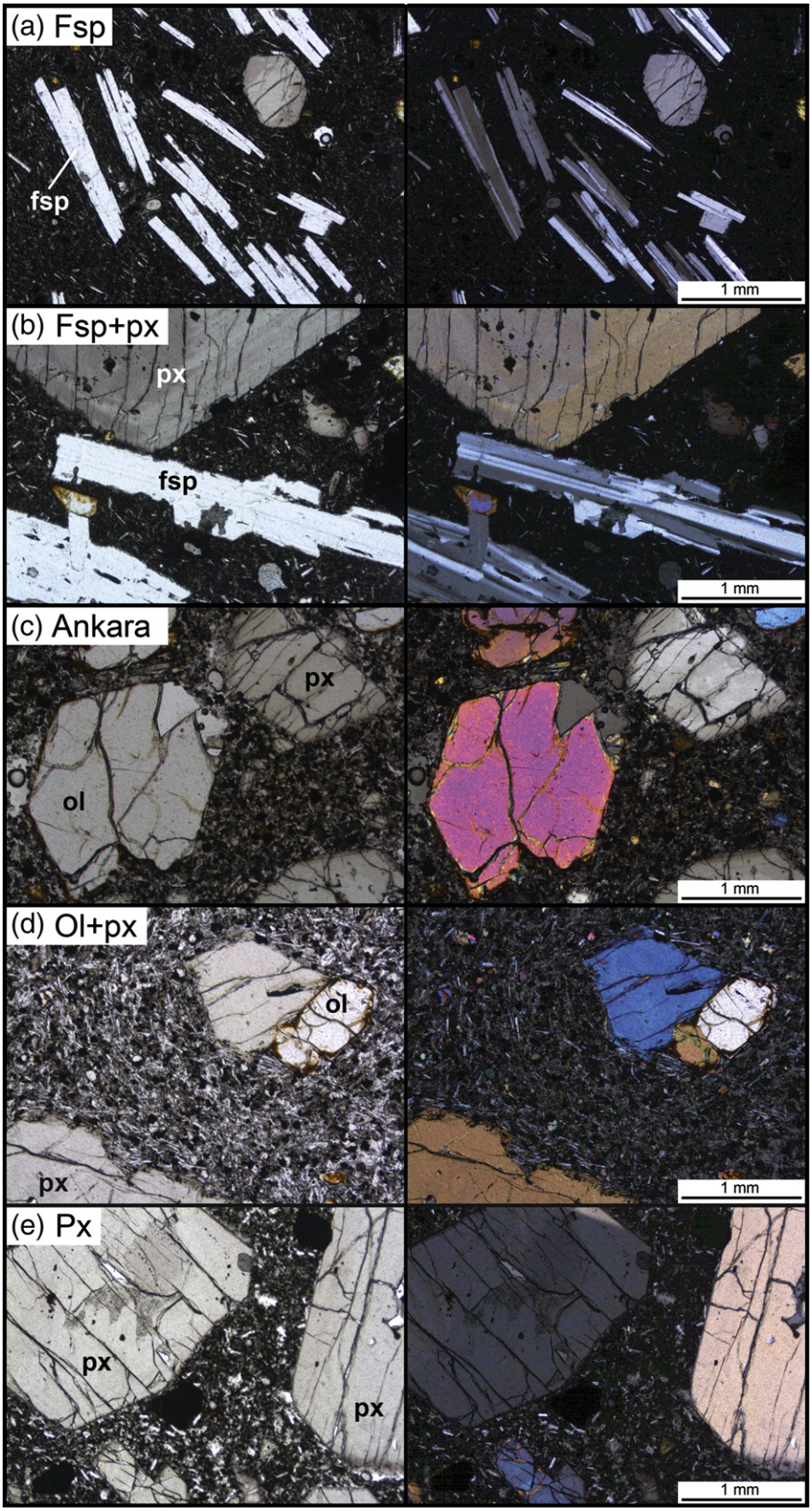

Fig. 2. Representative photomicrographs of the petrographic groups of dykes analysed in this study (aphyric types not shown). (a) Feldspar-phyric group, (b) feldspar and pyroxene–phyric group, (c) ankaramites, (d) olivine and pyroxene–phyric group, and (e) pyroxene–phyric group. Plane polarised view is shown on the left and cross polarised view on the right. Abbreviations: Fsp = feldspar, px = pyroxene, ol = olivine, ankara = ankaramite.

Table 1
Major and trace element compositions of dykes of the Northeast Rift Zone on Tenerife determined by XRF (only dykes for which isotopic analysis exists).

Sample:	NER-2	NER-3	NER-10	NER-12	NER-13	NER-18A	NER-29	NER-37A	NER-37W	NER-40	NER-46	NER-47	NER-57B
SiO_2	45.55	45.34	46.41	43.78	44.34	43.55	42.68	47.70	45.37	42.24	42.86	46.66	40.12
TiO_2	3.75	3.5	3.33	4.10	4.01	4.15	4.29	2.71	3.19	4.28	4.69	3.08	5.04
Al_2O_3	17.09	17.27	17.00	16.52	16.57	16.45	15.12	17.74	16.90	16.37	15.22	17.50	13.99
Fe_2O_3	12.24	11.28	11.57	14.01	13.81	14.30	15.38	10.25	11.69	13.84	16.28	10.92	16.13
MnO	0.17	0.20	0.19	0.18	0.18	0.17	0.18	0.21	0.23	0.18	0.18	0.19	0.17
MgO	4.57	4.03	4.38	4.91	4.51	4.88	5.84	3.66	4.29	5.72	5.33	4.18	6.56
CaO	9.66	9.45	9.01	10.50	8.84	9.89	12.34	8.33	9.32	10.50	9.72	8.78	11.87
Na_2O	3.76	4.99	4.63	3.63	4.40	3.92	2.76	5.24	4.17	2.65	3.65	4.44	3.31
K_2O	2.21	2.62	2.43	1.72	2.44	2.03	1.28	2.76	2.43	2.07	1.85	2.52	1.45
P_2O_5	0.80	1.09	1.01	0.76	1.18	0.84	0.61	1.02	1.27	0.97	0.76	1.09	0.79
Sum*	100.11	100.11	100.28	100.42	100.65	100.49	100.78	100.01	99.25	99.18	100.83	99.71	99.76
H_2O[a]	0.95	0.43	0.39	0.48	0.65	0.59	0.92	0.69	1.16	1.90	0.55	0.92	0.89
CO_2[a]	0.04	0.04	0	0.06	0.03	0.02	0.04	0.04	0.03	0.06	0.01	0.03	0.02
Co	65	52	54	75	71	71	85	60	73	69	50	56	83
Cr	–	–	–	–	50	27	–	–	–	43	–	–	50
Ni	14	–	–	10	20	32	37	–	–	35	52	–	51
V	291	235	243	317	292	350	399	187	224	323	416	215	397
Zn	106	124	122	116	117	117	111	130	130	114	128	118	127
Ce	115	147	172	100	149	109	90	188	170	124	102	135	80
La	35	84	61	55	43	41	22	86	78	24	44	85	34
Nb	93	136	119	82	112	94	67	149	140	113	83	130	95
Ga	27	23	26	26	23	30	26	29	27	28	27	24	29
Pb	17	14	9	11	17	10	16	10	8	11	10	11	14
Pr	8	17	16	9	11	10	–	16	16	11	9	17	9
Rb	69	69	69	43	57	51	34	79	68	53	46	68	45
Ba	555	712	651	536	666	561	402	750	694	654	467	700	511
Sr	1102	1242	1105	962	1150	985	872	1275	1332	1311	773	1161	904
Th	30	32	26	23	27	29	18	29	24	22	32	32	30
Y	22	31	26	26	27	26	25	29	29	31	28	30	24
Zr	391	540	507	347	525	376	301	587	556	463	366	517	401

Major elements are given as wt.% oxide; trace elements are given in ppm; '–' indicates that the analysis was below the detection limit. Sum* = total of major elements expressed as oxides.
[a]Volatiles measured by IR-photometry at Geomar.

1997). Canary Island magmatism is believed to involve melting predominantly of a HIMU-like mantle component, mixed with DMM and EM-1 components (e.g. Hoernle et al., 1991, 1995; Marcantonio et al., 1995; Widom et al., 1999; Simonsen et al., 2000; Geldmacher et al., 2001; Abratis et al., 2002; Demény et al., 2004; Gurenko et al., 2006, 2009, 2010; Day et al., 2009). Due to the various magmatic processes that primary ocean island magmas may undergo during ascent to the surface, they may not always faithfully record their source isotope signatures. Generally speaking, contamination by the ocean crust is widely believed to be small, due to the relatively thin crust through which ocean island magmas pass. Several studies have shown, however, that crustal assimilation in ocean island settings occurs to variable degrees (e.g. Marcantonio et al., 1995; Thirlwall et al., 1997; Harris et al., 2000; Gurenko et al., 2001; Hansteen and Troll, 2003; Wang and Eiler, 2008; Day et al., 2009). When assimilation takes place during magma storage within the pre-existing island edifice, recognition of crustal contamination becomes challenging. Elemental variations may not be useful indicators of contamination when the newly arriving magma and the existing island edifice are chemically similar (e.g. O'Hara, 1998; Wolff et al., 2000; Wiesmaier et al., 2012). Where the island edifice is compositionally heterogeneous due to the presence of differentiated (felsic) and variably altered erupted, sedimentary, and plutonic products, recognition of "island recycling" is aided by, e.g., oxygen isotopes, which are sensitive to alteration processes within the edifice (Taylor, 1968; Thirlwall et al., 1997; Garcia et al., 1998; Harris et al., 2000; Wolff et al., 2000; Hansteen and Troll, 2003; Wang and Eiler, 2008). Assimilation of hydrothermally altered material may also perturb the $^{87}Sr/^{86}Sr$ of the ascending magmas, but should not substantially alter their Nd–Pb isotope composition (cf. Staudigel et al., 1995; Gaffney et al., 2005). Therefore, an approach that utilises stable (O) and radiogenic (Sr–Nd–Pb) isotope systems in ocean island basalts, and indeed in other tectonic settings too, has the potential to unravel the effects of shallow-level crustal differentiation and identify the mantle components that the magmas have ultimately derived from (cf. Demény et al., 2004; Peccerillo et al., 2004; Gaffney et al., 2005; Day et al., 2009).

In this paper, we build on previous paleomagnetic and structural studies of a suite of dykes from the Northeast Rift Zone (NERZ) on Tenerife, known locally as the "Cumbre Dorsal", (Delcamp et al., 2010, 2012; Carracedo et al., 2011). These previous papers describe the field characteristics of the NERZ dykes, which effectively represent the upper section of the magma plumbing system that fed a Pleistocene rift, with an interval of dyke intrusion occurring between 0.99 Ma and 0.56 Ma (Delcamp et al., 2010). We selected 83 dykes for major and trace element analyses and a subset of 27 dykes for analysis of oxygen isotopes and 20 for Sr–Nd–Pb isotopes. Some radiogenic isotope data have been reported previously for lavas of the NERZ, but they are very few (Simonsen et al., 2000, $n=3$). Our study therefore represents the first detailed isotopic investigation of a Canary Island rift zone wherein we identify and attempt to quantify late-stage processes to resolve the underlying mantle isotope signatures. Our objective is to provide insights into the origin and evolution of rift zone magmas and to test for genetic links between various episodes of island development (e.g. the shield building and post-shield stages).

2. Geological framework

2.1. General geology

Tenerife is one of the central islands of the Canary Archipelago, located ca. 300 km off the NW coast of Africa (Fig. 1a). The ages of the oldest exposed volcanic rocks in the Canaries decrease towards the west, younging from >20 Ma on the eastern islands to ca. 1 Ma on the western islands (McDougall and Schmincke, 1976; LeBas et al., 1986; Carracedo et al., 1998; Guillou et al., 2004). A model of lithospheric fracturing has been suggested for the origin of the Canaries by some authors (e.g. Anguita and Hernán, 1975, 2000), however, a mantle

NER-61	NER-65	NER-66	NER-70	NER-70A	NER-73	NER-77	NER-81	G2-D11	G2-D19	G2-D20	G2-D29	LC-7	LO-25
43.96	52.93	52.07	47.89	43.73	50.04	43.69	42.11	45.36	42.39	47.96	44.30	58.65	57.19
4.00	1.60	1.81	2.86	4.10	2.36	2.36	4.48	3.52	3.95	2.99	4.17	0.61	1.22
16.85	19.30	19.02	18.77	16.71	18.33	8.72	14.61	16.86	11.98	17.26	16.52	20.44	19.15
11.42	6.43	7.09	9.18	12.03	9.01	13.52	14.86	11.42	14.68	11.07	13.20	3.16	5.27
0.19	0.19	0.19	0.18	0.18	0.21	0.17	0.17	0.17	0.17	0.18	0.17	0.18	0.24
4.66	1.60	1.86	2.94	4.92	2.92	18.32	6.72	4.35	10.03	4.22	5.58	0.48	1.08
10.16	5.40	5.84	7.96	10.42	7.43	10.88	11.71	9.60	11.88	8.32	9.90	2.11	4.21
4.93	7.06	7.12	5.82	4.29	5.41	1.47	2.74	3.61	2.18	4.31	3.49	7.31	6.60
2.56	3.61	3.56	3.05	2.28	2.45	0.64	1.34	1.93	1.27	2.18	1.72	4.57	3.19
1.11	0.41	0.50	0.67	1.07	0.80	0.35	0.82	1.01	0.55	0.73	0.79	0.09	0.27
100.18	98.96	99.48	99.68	100.09	99.33	100.50	99,88	98.14	99.42	99.50	100.12	97.92	98.80
0.44	0.63	0.44	0.86	0.65	0.72	0.54	1.33	1.03	1.43	0.89	0.88	1.27	0.77
0.04	0.00	0.03	0.03	0.01	0.05	0.04	0.04	1.56	0.52	0.61	0.24	0.64	0.02
53	33	60	49	56	44	110	76	41	80	45	61	46	40
–	–	–	–	–	–	1044	89	–	470	–	–	–	–
–	–	–	–	–	–	582	59	–	203	–	11	–	–
268	112	120	182	278	144	253	377	238	350	227	273	28	33
118	114	117	109	115	116	89	113	110	101	116	105	100	123
135	187	186	177	138	165	50	109	113	64	133	119	187	209
68	76	106	90	67	84	–	34	39	–	54	31	110	114
133	168	172	163	126	135	36	73	85	55	92	78	173	200
25	27	28	28	25	23	17	28	23	22	25	24	29	24
15	7	22	6	10	–	10	11	17	12	9	10	18	16
11	14	20	16	13	18	–	9	10	–	11	10	20	25
65	121	120	80	58	66	20	35	48	36	56	39	154	89
686	1060	994	751	660	746	246	455	551	383	600	518	1068	997
1215	1426	1396	1280	1199	1254	434	883	1045	750	885	975	592	1197
27	33	33	32	33	33	27	26	32	24	29	28	41	36
30	17	22	28	31	30	15	27	28	19	24	26	7	30
510	758	767	615	505	466	135	335	397	233	383	346	724	656

plume origin is currently most widely accepted, and is supported by the age progression of the islands and the presence of a low seismic velocity zone beneath the Canaries which can be traced to about 2800 km depth (Hoernle et al., 1995; Carracedo et al., 1998; Montelli et al., 2004; Geldmacher et al., 2005).

An overview of the volcanic evolution of Tenerife is presented by Ancochea et al. (1990). The geochronology of the old shield basalt massifs has been established in detail by Thirlwall et al. (2000) and Guillou et al. (2004). These works demonstrate that shield building on Tenerife was rapid, beginning with construction of the Central Roque del Conde Shield (11.9–8.9 Ma), followed by the Teno (6.2–5.6 Ma) and Anaga (4.9–3.9 Ma) volcanoes (Guillou et al., 2004; Walter et al., 2005) (Fig. 1b). Initiation of the NERZ from the Central Shield in the Miocene–Pliocene has been suggested by Guillou et al. (2004) and Carracedo et al. (2011). After the shield building phase, a period of quiescence followed after which the Las Cañadas phase of volcanism began. The subsequent evolution of the Las Cañadas central edifice occurred coeval to the main growth stage of the Pleistocene NERZ (Ancochea et al., 1990; Carracedo et al., 2007, 2011). The Las Cañadas volcano culminated in a period of major instability, characterised by vertical caldera collapses and a major lateral collapse (the Icod landslide), the latter at ca. 200 ka ago (Martí et al., 1997; Edgar et al., 2002; Carracedo et al., 2007). This initiated the latest phase of activity on Tenerife, the construction of the central Teide–Pico Viejo complex within the Icod landslide scar and continued activity on the NE and NW rift zones (Carracedo et al., 2007, 2011).

2.2. Field area and sample selection

The North East Rift Zone (NERZ) on Tenerife underwent rapid intrusion and construction between ca. 1.1 and 0.56 Ma (Delcamp et al., 2010; Carracedo et al., 2011). The age determinations for this period of growth overlap with three successive mass wasting events on both sides of the rift, forming the Micheque, Güímar (both at ca. 0.83 Ma), and La Orotava (ca. 0.69 Ma) landslide depressions (Carracedo, 1994; Watts and Masson, 1995; Carracedo et al., 2011) (Fig. 1b). Detailed overview of the evolution of the rift zone and a detailed structural analysis from field relations of the dykes are given by Carracedo et al. (2011) and Delcamp et al. (2010, 2012). The present paper investigates the geochemical evolution of the NERZ on the basis of 83 whole rock dyke samples obtained mainly by systematic sampling of well exposed and accessible outcrops along the road section TF-24, which follows the topography of the NERZ (the "Cumbre Dorsal"; $n=65$; see Fig. 1c and d). We also sampled dykes in two water tunnels ("galerías") that are constructed within the old Miocene rift zone interior ($n=7$; Fig. 1c), as well as along two trails on the crest of the La Orotava collapse scar ("La Orotava", $n=8$ and "La Crucita", $n=3$). Weathered surfaces were removed in the field, and in some cases cored samples were obtained by drilling, yielding fresh samples of dyke interiors. Sample locations, petrographic and TAS classification, and paleomagnetic data are provided in Table S1.

3. Petrography of the NERZ dykes

The dykes of the NERZ, although almost exclusively basaltic, display wide petrographic variability. Aphyric to weakly phyric texture is most common along the rift zone (32 out of 83 samples in this study), but we have also identified five other petrographic groups as described in Delcamp et al. (2010, 2012) and in this study. Based on a set of >50 thin sections, the following six groups have been identified (Fig. 2): 1) aphyric group; these dykes are largely phenocryst free or only weakly-phyric. Occasional small crystals (<1 mm) of pyroxene and feldspar are observed in a microcrystalline, sometimes glassy, groundmass. Micro-phenocrysts generally constitute less than 5% of the rock volume. 2) Feldspar-rich group ("fsp" dykes); these dykes contain feldspar as the dominant phenocryst phase, occupying 40 to 50% of the rock volume.

Table 2
Trace and rare earth element and Sr–Nd–Pb isotope composition of selected dykes of the Northeast Rift Zone on Tenerife.

Sample	NER-12	NER-18A	NER-18A[a]	NER-29	NER-37A	NER-37W	NER-37W[a]	NER-40	NER-47	NER-47[a]
Petro.	fsp	fsp + px	fsp + px	Aphyric	ol + px	Ankara	Ankara	px	Ankara	Ankara
TAS	Basanite	Basanite	Basanite	Basanite	Basanite	Basanite	Basanite	Basanite	Basanite	Basanite
Li	5.56	6.91	6.80	2.93	6.15	11.52	11.64	4.23	6.34	6.18
Be	2.32	2.68	2.61	2.11	3.84	1.16	1.30	2.83	0.85	0.84
Sc	9.95	12.34	12.11	8.95	3.31	10.31	10.34	5.78	7.24	7.20
Ti	25459.00	27529.00	27314.00	26827.00	16557.00	16236.00	16132.00	24170.00	8198.00	8266.00
V	337.66	406.91	403.73	463.20	196.39	159.17	158.88	328.14	89.20	88.40
Cr	2.39	25.54	25.11	5.09	0.31	2.58	2.81	35.08	0.32	0.37
Co	81.76	85.68	84.95	102.14	71.79	19.15	19.24	67.83	8.16	8.32
Ni	26.31	55.92	55.86	54.96	2.66	6.00	6.04	53.87	3.39	3.50
Cu	107.89	128.71	128.14	194.52	29.70	21.78	21.89	85.06	12.48	12.41
Zn	121.79	153.44	153.18	123.91	116.16	95.62	95.26	125.46	45.60	45.72
Ga	20.70	23.67	23.55	18.28	24.76	17.71	17.75	18.23	13.71	13.87
Rb	33.01	49.49	48.64	19.58	62.03	58.11	57.19	31.32	42.15	41.48
Sr	724.64	843.63	837.88	577.67	739.43	1205.85	1202.99	731.34	900.39	895.86
Y	22.21	24.37	24.16	13.73	19.74	23.96	23.98	16.92	16.37	16.16
Zr	342.63	393.62	388.17	247.62	611.46	486.06	481.84	428.03	367.90	364.67
Nb	87.16	100.04	99.81	73.96	126.01	130.99	133.61	91.51	82.95	84.48
Mo	0.47	0.58	0.55	0.47	1.11	0.39	0.41	0.71	0.08	0.07
Cd	0.05	0.11	0.10	0.08	0.77	0.07	0.05	0.15	0.04	0.05
In	0.18	0.18	0.18	0.20	0.19	0.17	0.17	0.18	0.14	0.15
Sn	1.35	1.45	1.38	1.75	1.38	1.85	1.85	0.89	1.07	1.04
Sb	0.07	0.09	0.09	0.07	0.19	0.05	0.05	0.14	0.05	0.04
Cs	0.17	0.36	0.35	0.11	0.32	0.44	0.42	0.15	0.28	0.26
Ba	416.17	493.33	491.04	347.95	442.52	676.93	676.52	481.90	530.41	525.01
La	38.53	49.71	49.89	31.38	47.96	25.62	25.72	45.41	18.25	18.06
Ce	104.78	127.36	126.86	97.31	162.12	53.94	54.25	131.91	43.34	43.04
Pr	9.60	11.51	11.54	8.71	10.76	7.42	7.37	10.12	5.46	5.36
Nd	38.51	44.98	44.09	35.80	40.27	31.53	31.00	38.99	23.15	22.56
Sm	7.24	8.35	8.23	7.05	7.01	6.75	6.82	6.79	5.01	4.98
Eu	2.37	2.57	2.64	2.15	2.22	2.76	2.87	2.06	2.03	2.08
Tb	0.89	0.98	0.97	0.78	0.81	0.89	0.88	0.75	0.62	0.61
Gd	6.31	7.12	6.82	5.86	5.65	6.12	6.00	5.57	4.44	4.30
Dy	4.57	5.09	5.00	4.06	4.01	4.89	4.66	3.97	3.45	3.31
Ho	0.79	0.85	0.87	0.67	0.70	0.82	0.83	0.66	0.60	0.59
Er	2.00	2.17	2.14	1.65	1.78	2.17	2.03	1.57	1.61	1.55
Tm	0.25	0.28	0.26	0.20	0.24	0.30	0.29	0.21	0.22	0.22
Yb	1.57	1.63	1.69	1.12	1.42	1.87	1.90	1.19	1.33	1.37
Lu	0.20	0.23	0.22	0.14	0.18	0.26	0.26	0.15	0.21	0.20
Hf	7.08	7.79	7.80	5.52	11.29	9.25	9.23	8.05	7.48	7.55
Ta	5.86	6.79	6.81	5.71	9.69	7.87	7.80	7.23	5.41	5.33
W	175.13	124.81	138.75	172.29	221.22	206.19	217.38	73.59	0.37	0.42
Tl	0.07	0.06	0.10	0.06	0.35	0.04	0.06	0.10	0.06	0.08
Pb	1.50	2.03	2.01	1.50	3.23	1.94	1.95	2.36	1.00	0.98
Bi	0.01	0.02	0.02	0.02	0.02	0.01	0.01	0.02	0.21	0.22
Th	3.94	5.38	5.46	1.97	6.21	5.49	5.72	4.90	1.98	2.02
U	1.16	1.46	1.47	1.02	2.98	1.82	1.84	2.04	0.77	0.76
$^{87}Sr/^{86}Sr$	0.703093	0.703096	–	0.703087	0.703092	0.703126	–	0.703111	0.703129	–
2SE	0.000009	0.000009	–	0.000009	0.000008	0.000006	–	0.000009	0.000007	–
$^{143}Nd/^{144}Nd$	0.512854	0.512894	–	0.512966	0.512876	0.512892	–	0.512846	0.512928	–
2SE	0.000030	0.000028	–	0.000024	0.000022	0.000028	–	0.000026	0.000036	–
$^{206}Pb/^{204}Pb$	19.706	19.774	–	19.714	19.810	19.802	–	19.779	–	–
2SE	0.002	0.002	–	0.003	0.001	0.003	–	0.001	–	–
$^{207}Pb/^{204}Pb$	15.611	15.616	–	15.619	15.625	15.618	–	15.619	–	–
2SE	0.002	0.002	–	0.003	0.002	0.003	–	0.002	–	–
$^{208}Pb/^{204}Pb$	39.580	39.676	–	39.600	39.693	39.664	–	39.664	–	–
2SE	0.003	0.004	–	0.006	0.003	0.005	–	0.003	–	–

Petro. = petrographic group; see text for descriptions.aDenotes ICP-MS duplicate analysis.

Rare clinopyroxene, olivine, and Fe–Ti oxide crystals may be present with each constituting less than 10% of the rock volume. 3) Feldspar- and pyroxene-rich group ("fsp + px" dykes); the main phenocryst phases in these dykes are feldspar and pyroxene occupying 40 to 50% of the rock volume, with feldspar generally more abundant than pyroxene. Minor olivine and Fe–Ti oxides may be present at up to 10% of the rock volume. 4) Ankaramite group ("ankara"); these dykes are easily recognisable in the field due to their high crystal content and conspicuous, large (up to 2 cm across) olivine and pyroxene phenocrysts occupying 40 to 60% or more of the rock volume. Minor phenocryst phases include amphibole and Fe–Ti oxides. Ankaramite groundmass ranges from microcrystalline to Fe–Ti oxide-rich. 5) Olivine- and pyroxene-rich group ("ol + px" dykes); these dykes are mineralogically similar to the ankaramite group. However, they are much less porphyritic than the ankaramites, with crystal contents ranging from 5 to 35% of the rock volume. Phenocrysts are a few mm in size, making them

NER-57B	NER-57B[a]	NER-61	NER-65	NER-65[a]	NER-66	NER-70	NER-70A	NER-70A[a]	NER-77	NER-77[a]
Ankara	Ankara	Aphyric	fsp	fsp	fsp + px	px	px	px	Ankara	Ankara
Basanite	Basanite	Basanite	Tephri-phonolite	Tephri-phonolite	Tephri-phonolite	Phono tephrite	Basanite	Basanite	Picro-basalt	Picro-basalt
4.30	4.26	4.68	6.56	6.85	17.90	4.12	6.72	6.69	3.04	3.02
1.23	1.32	2.79	5.77	5.66	6.59	3.70	2.62	2.79	0.59	0.59
22.62	22.53	4.96	1.43	1.56	4.06	1.88	7.60	7.52	31.53	31.53
28620.00	28195.00	24549.00	10799.00	11147.00	12896.00	16868.00	23837.00	23811.00	9366.00	9366
341.27	338.56	289.28	119.19	120.33	134.44	176.45	284.88	283.61	215.70	215.70
36.54	35.98	0.64	1.79	1.84	3.43	2.90	0.91	0.79	1073.82	1073.82
41.34	41.22	67.21	43.42	44.13	86.28	59.44	62.95	62.88	57.29	57.29
46.50	46.41	7.71	3.26	3.29	4.02	8.66	12.23	12.18	347.02	347.02
44.31	43.90	42.33	22.73	22.97	20.09	35.03	44.18	43.98	51.82	51.82
133.38	132.18	141.34	103.01	104.22	126.12	87.40	126.33	125.95	88.99	88.99
17.19	16.95	19.91	27.20	27.53	31.15	21.02	19.87	19.57	11.06	11.06
19.35	19.12	52.59	61.94	61.86	97.39	57.75	44.20	44.75	9.74	9.74
743.28	734.23	783.54	522.59	532.34	1346.29	412.85	891.03	888.13	342.29	342.29
20.00	19.78	17.26	11.85	12.06	36.20	8.95	25.74	25.71	11.02	11.02
342.40	339.83	486.12	890.17	899.24	923.10	583.15	468.41	471.51	142.54	142.54
96.06	97.58	95.40	201.21	207.28	205.05	128.67	97.41	96.45	38.28	38.28
0.41	0.39	0.85	0.76	0.76	1.04	1.13	0.51	0.53	0.28	0.28
0.03	0.04	0.23	0.18	0.17	0.11	0.14	0.10	0.12	0.04	0.04
0.19	0.22	0.21	0.15	0.16	0.17	0.14	0.20	0.21	0.12	0.12
2.17	2.17	0.94	2.38	2.50	2.39	0.92	1.23	1.27	0.64	0.64
0.05	0.05	0.15	0.27	0.27	0.28	0.18	0.11	0.11	0.02	0.02
0.14	0.12	0.25	0.52	0.51	1.20	0.24	0.26	0.26	0.06	0.06
467.32	464.31	453.56	520.94	531.66	984.64	279.47	527.36	522.52	204.36	204.36
21.02	20.88	47.09	36.39	37.01	105.72	23.31	57.22	56.44	7.89	7.89
51.30	50.73	147.79	108.89	110.41	191.62	83.90	149.26	148.99	18.64	18.64
7.09	7.10	10.41	6.45	6.52	19.15	4.99	13.60	13.50	2.64	2.64
31.69	30.92	39.58	22.08	22.07	66.77	18.31	52.56	53.37	12.28	12.28
7.38	6.98	7.03	3.44	3.56	10.77	3.18	9.87	9.90	3.05	3.05
2.51	2.63	2.11	1.07	1.11	3.36	0.96	3.09	2.98	1.24	1.24
0.86	0.88	0.73	0.41	0.42	1.21	0.35	1.13	1.12	0.43	0.43
6.39	6.41	5.68	2.70	2.77	8.66	2.45	7.92	8.05	2.90	2.90
4.75	4.50	3.85	2.24	2.17	6.66	1.88	5.66	5.83	2.32	2.32
0.78	0.78	0.64	0.39	0.40	1.21	0.32	0.97	0.95	0.41	0.41
1.93	1.85	1.55	1.08	1.12	3.20	0.84	2.38	2.41	1.05	1.05
0.25	0.24	0.20	0.15	0.15	0.47	0.11	0.29	0.30	0.14	0.14
1.41	1.42	1.10	0.99	1.06	2.80	0.64	1.80	1.72	0.86	0.86
0.19	0.20	0.14	0.14	0.15	0.41	0.08	0.23	0.23	0.12	0.12
7.30	7.44	9.13	14.89	15.06	15.87	9.98	9.16	8.85	2.99	2.99
6.05	5.99	8.39	8.47	8.54	10.35	9.18	7.70	7.64	2.84	2.84
127.42	191.48	88.44	148.62	157.15	260.59	103.96	90.58	79.79	122.60	122.60
0.03	0.04	0.18	0.30	0.44	0.15	0.25	0.22	0.13	0.01	0.01
1.14	1.12	2.54	4.44	4.45	5.68	2.98	2.33	2.29	0.62	0.62
0.05	0.05	0.02	0.03	0.03	0.02	0.02	0.03	0.03	0.02	0.02
2.50	2.56	5.38	5.13	5.36	14.54	2.77	6.24	6.06	1.30	1.30
0.94	0.95	2.28	3.00	3.14	4.33	2.57	1.87	1.82	0.46	0.46
0.703137	–	0.703099	0.703101	–	0.703077	0.703092	0.703091	–	0.703152	–
0.000010	–	0.000006	0.000009	–	0.000008	0.000009	0.000008	–	0.000007	–
0.512891	–	0.512815	0.512897	–	0.512802	0.512869	0.512947	–	0.512958	–
0.000022	–	0.000022	0.000014	–	0.000030	0.000016	0.000022	–	0.000028	–
19.833	–	19.838	–	–	19.796	19.796	19.779	–	19.656	–
0.003	–	0.003	–	–	0.002	0.001	0.003	–	0.012	–
15.622	–	15.625	–	–	15.624	15.623	15.619	–	15.624	–
0.002	–	0.003	–	–	0.002	0.002	0.003	–	0.010	–
39.713	–	39.726	–	–	39.700	39.694	39.667	–	39.589	–
0.005	–	0.005	–	–	0.003	0.002	0.007	–	0.025	–

(continued on next page)

substantially smaller than in the ankaramites. The groundmass is generally rich in plagioclase and Fe–Ti oxides. 6) Pyroxene-rich group ("px" dykes); they contain clinopyroxenes between 5 and 30% of the rock volume. Minor phenocryst phases include amphibole and Fe–Ti oxides at less than 10% of the rock volume. Note that the petrographic groupings of dykes do not have a specific paleomagnetic polarity (Delcamp et al., 2010), i.e., the petrographic groups did not erupt in distinct pulses, but probably largely concurrently over the lifetime of the rift. A list of samples, their petrographic grouping, and location is provided in Table S1.

4. Analytical methods

4.1. Major and trace elements (XRF)

Major and trace elements were determined on whole rock powders by X-ray Fluorescence (XRF) at IFM-GEOMAR, Kiel, Germany. Fused glass beads were analysed using an automated Philips PW1480 X-ray spectrometer following the method given in Abratis et al. (2002) and references therein. All analyses were carried out using a Rh X-ray

Table 2 (*continued*)

Sample	NER-81	NER-81[a]	G2-D11	G2-D19	G2-D19[a]	G2-D20	LC-7	LC-7[a]	LO-25
Petro.	ol + px	ol + px	fsp	fsp + px	fsp + px	Aphyric	fsp + px	fsp + px	Aphyric
TAS	Basanite	Basanite	Basanite	Basanite	Basanite	Basanite	Trachyte	Trachyte	Trachy-andesite
Li	5.37	5.45	8.72	9.07	9.09	7.34	19.05	18.88	15.52
Be	1.81	1.97	2.58	1.68	1.63	2.91	6.87	7.10	5.24
Sc	19.59	19.27	15.54	34.80	34.89	8.44	1.07	0.88	1.47
Ti	28,429	28,596	24,845	24,899	24,648	20,625	3940	3869	7500
V	430.65	431.79	259.33	413.86	411.34	252.75	33.88	33.92	28.45
Cr	106.53	104.96	0.63	573.03	573.84	12.63	0.79	0.77	0.38
Co	80.96	81.49	47.66	91.24	90.26	61.95	71.33	71.98	50.61
Ni	77.35	76.70	3.69	229.51	228.15	9.95	0.61	0.71	0.68
Cu	123.03	122.65	28.42	157.25	156.91	29.10	2.78	2.77	5.35
Zn	129.08	128.83	131.48	130.88	132.22	115.47	83.24	82.14	98.82
Ga	21.87	21.75	25.65	23.52	23.58	23.92	28.77	28.52	24.02
Rb	27.54	27.78	50.78	38.41	37.54	50.88	81.08	82.35	29.97
Sr	765.73	767.23	1174.20	834.65	831.42	684.77	281.98	275.26	758.91
Y	24.31	24.48	42.04	30.40	30.11	22.39	12.23	12.21	33.87
Zr	305.38	309.44	433.93	259.74	257.14	434.04	872.69	883.97	730.25
Nb	85.44	84.30	108.12	67.01	67.72	99.14	193.21	191.96	215.74
Mo	0.63	0.61	0.52	0.34	0.36	0.82	1.62	1.67	1.49
Cd	0.09	0.11	0.11	0.13	0.11	0.13	0.18	0.19	0.18
In	0.23	0.22	0.23	0.21	0.23	0.22	0.10	0.09	0.16
Sn	2.39	2.41	2.54	2.15	2.02	1.46	1.72	1.80	2.80
Sb	0.08	0.08	0.21	0.04	0.04	0.08	0.34	0.34	0.20
Cs	0.24	0.24	0.62	0.33	0.31	0.43	1.14	1.16	0.51
Ba	450.62	454.35	576.40	469.46	465.84	453.79	792.63	793.91	740.38
La	48.38	48.32	70.08	40.42	40.26	43.01	59.39	59.03	88.94
Ce	119.27	119.87	150.92	88.79	88.48	133.58	78.01	78.18	168.12
Pr	13.03	13.06	17.64	11.59	11.38	10.33	6.47	6.44	17.57
Nd	52.66	53.94	70.74	50.08	48.38	39.07	17.21	17.66	62.35
Sm	10.37	10.45	13.71	10.64	10.44	7.05	2.23	2.16	10.17
Eu	3.29	3.23	4.36	3.33	3.46	2.18	0.70	0.69	2.95
Tb	1.17	1.21	1.59	1.29	1.28	0.83	0.28	0.29	1.10
Gd	8.46	8.78	11.61	9.59	9.19	5.92	1.65	1.68	7.59
Dy	5.94	6.02	8.35	6.55	6.41	4.38	1.64	1.66	6.09
Ho	1.01	1.01	1.47	1.08	1.07	0.77	0.36	0.36	1.13
Er	2.52	2.49	3.68	2.63	2.53	2.01	1.17	1.17	3.08
Tm	0.30	0.31	0.48	0.32	0.31	0.27	0.19	0.19	0.46
Yb	1.82	1.77	2.92	1.82	1.86	1.68	1.38	1.34	2.69
Lu	0.23	0.24	0.39	0.24	0.24	0.23	0.22	0.23	0.37
Hf	6.55	6.36	8.76	5.97	6.11	8.31	13.56	13.38	13.65
Ta	5.50	5.65	6.43	4.39	4.26	6.75	6.85	6.95	12.23
W	81.20	73.67	104.97	120.20	132.64	175.78	134.37	120.93	136.10
Tl	0.12	0.08	0.15	0.10	0.12	0.29	0.86	0.58	0.33
Pb	1.72	1.78	2.41	1.21	1.18	2.84	4.68	4.70	3.42
Bi	0.01	0.02	0.02	0.02	0.02	0.03	0.05	0.05	0.03
Th	3.79	3.69	7.33	3.39	3.51	4.76	12.69	12.45	11.58
U	1.32	1.29	2.01	0.72	0.70	2.13	4.00	3.97	2.64
$^{87}Sr/^{86}Sr$	0.703078	–	0.703084	0.703081	–	0.703205	0.703161	–	0.703079
2SE	0.000008	–	0.000008	0.000010	–	0.000008	0.000009	–	0.000009
$^{143}Nd/^{144}Nd$	0.512808	–	0.512872	0.512904	–	0.512893	0.512898	–	0.512870
2SE	0.000028	–	0.000036	0.000024	–	0.000022	0.000022	–	0.000026
$^{206}Pb/^{204}Pb$	19.704	–	19.680	19.591	–	19.669	19.740	–	19.779
2SE	0.004	–	0.003	0.005	–	0.001	0.002	–	0.001
$^{207}Pb/^{204}Pb$	15.603	–	15.610	15.603	–	15.636	15.616	–	15.619
2SE	0.004	–	0.003	0.005	–	0.002	0.003	–	0.002
$^{208}Pb/^{204}Pb$	39.581	–	39.563	39.416	–	39.586	39.608	–	39.628
2SE	0.008	–	0.006	0.011	–	0.003	0.004	–	0.003

tube. Water and CO_2 contents were determined by IR photometry, also at IFM-GEOMAR.

4.2. Oxygen isotopes

On the basis of petrography and the major element data, 27 dyke samples were selected for whole rock oxygen stable isotope analysis, spanning the range of compositions observed. All oxygen isotope data were obtained at the Department of Geological Sciences, University of Cape Town (UCT) following the procedure given in Vennemann and Smith (1990) and Fagereng et al. (2008). Oxygen was released by reacting ca. 10 mg of un-leached sample powder dried at 50 °C with ClF_3 at 550 °C for at least 4 h in conventional Ni reaction vessels. The liberated O_2 was then converted to CO_2 using a hot platinized carbon rod and captured in a break-seal glass tube under vacuum. The CO_2 gas was then analysed using a DeltaXP mass spectrometer in

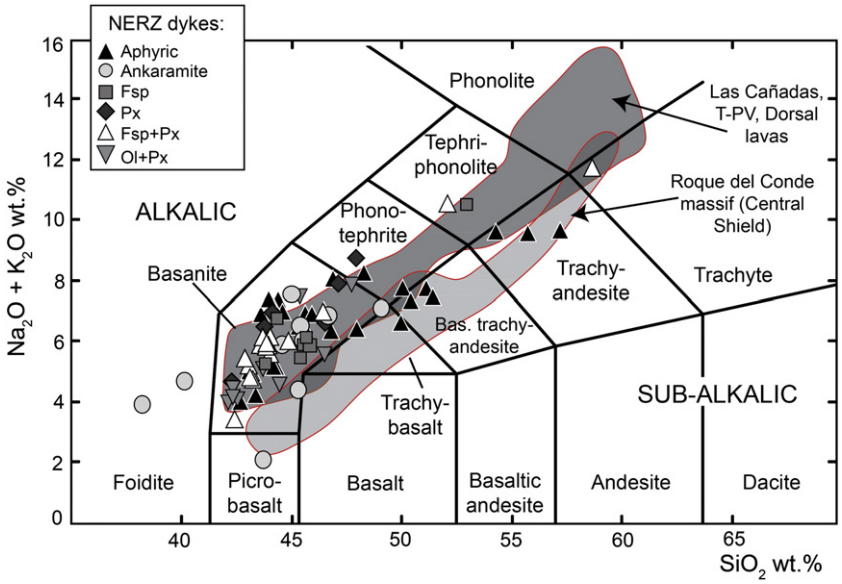

Fig. 3. Total alkalis versus silica (TAS) plot for dykes of the North East rift zone (NERZ) with boundaries drawn after Irvine and Baragar (1971) and nomenclature after Le Maitre et al. (1989). Symbols correspond to the petrographic groupings of the NERZ. Shaded fields are drawn using data for the Central Shield (Roque del Conde) after Thirlwall et al. (2000) and for the Las Cañadas volcano, the Teide–Pico Viejo complex (T–PV), and lavas from the NERZ after Ablay et al. (1998) and Neumann et al. (1999).

dual inlet mode. The results are reported in standard δ-notation relative to the SMOW (Standard Mean Ocean Water) scale, using the internal NBS-28 quartz standard ($\delta^{18}O = 9.64‰$) to normalise the raw data. In practice, the difference between the raw and normalised data was less than ca. 0.5‰. During the course of this study, the analytical error based on multiple analyses of the standard was ca. ± 0.1‰ (1σ). Pyroxene and olivine phenocryst separates from six dyke samples were additionally analysed by laser fluorination at UCT. Full analytical details for the laser line are given in Harris and Vogeli (2010). Measured values of the UCT internal standard MON GT (Harris et al., 2000) were used to normalise the raw data and correct for drift in the reference gas. The average difference in $\delta^{18}O$ values of duplicates of MON GT analysed during this study was 0.14‰, and corresponds to a 2σ value of 0.19‰.

4.3. Trace and rare earth elements (ICP-MS)

Each sample was digested using conventional HF–HCl–HNO_3 dissolution techniques in clean Teflon beakers. The ankaramite samples were the most prone to alteration and were in addition leached with HCl prior to dissolution. Samples were precisely diluted 4000–5000 times in 5% HNO_3 before inductively coupled mass spectrometry (ICP-MS) analysis. Analysis was carried out on a Thermo X-Series II Quadrupole ICP-MS at the Vrije Universiteit (VU) Amsterdam, Netherlands, following the standard procedure and instrument settings given in Eggins et al. (1997). Instrumental drift and reproducibility were monitored using repeated measurements of the BHVO-2 and BCR-2 geological reference materials. Analytical precision was better than 10% for all elements. The analyses of the BHVO-2 standards processed with the samples in this study are provided in Table S2.

4.4. Strontium isotope analysis (TIMS)

Strontium separation was performed using conventional Sr Spec cation exchange chromatography (Pin et al., 1994). Strontium isotope measurements were performed on a Finnigan MAT 262 TIMS system operating in static mode at the VU Amsterdam. Instrumental mass fractionation was corrected by normalising to $^{86}Sr/^{88}Sr = 0.1194$ using an exponential correction law. Long-term replicate analyses of NBS 987 at the VU gave a mean $^{87}Sr/^{86}Sr$ value of 0.710251 ± 9 (2SE, $n = 154$) and $^{84}Sr/^{86}Sr$ value of 0.056502 ± 5 (2SE, $n = 118$) over the period spanning May 2009 to December 2010. Measurements of NBS 987 made during the course of this study are within error of the long term reproducibility at the VU. Four BHVO-2 standards were processed with the samples and give an average $^{87}Sr/^{86}Sr$ ratio of 0.703445 ± 9 (2SE), compared to the average value reported by Raczek et al. (2003) of 0.703435 (see Table S3). Procedural blank values at the VU are typically ≤100 pg, which is negligible when compared to the 500 ng Sr loaded per sample. Thus, blank corrections were not made.

4.5. Neodymium and lead isotope analyses

Neodymium separation was carried out as a two column procedure, utilising conventional TRU Spec and LN Spec cation exchange chromatography (e.g. Pin et al., 1994). Lead separation was carried out using quartz columns (0.15 ml) filled with AGIx8 200–400 mesh (Elburg et al., 2005). Neodymium and Pb isotopes were analysed at the VU Amsterdam using a Finnigan Neptune multi collector ICP-MS (MC-ICP-MS). The method used to measure Nd isotope ratios is given in Luais et al. (1997). During the course of this study, repeat analysis of the CIGO internal standard gave a mean $^{143}Nd/^{144}Nd$ ratio of 0.511342 ± 13 (2SE, $n = 60$). This agrees with previous measurements by TIMS of the CIGO standard by Davies et al. (2006) of 0.511342 ± 7 (2SE, $n = 18$). Repeated analyses ($n = 4$) of the international geological reference standard BHVO-2 (procedural standard) gave a mean $^{143}Nd/^{144}Nd$ ratio of 0.512992 ± 49 (2SE). This agrees within error with the value reported in Weis et al. (2006). Lead isotopes were analysed using the method of standard-sample bracketing. Full details of the method used, the instrument settings, analytical reproducibility and data reduction are given in Elburg et al. (2005). Note that the instrument settings given by Elburg et al. (2005) were optimised between sessions, reflecting the sensitivity of the MC-ICP-MS to daily variations in tuning and atmospheric conditions. During the course of this study repeated analysis of the NIST (NBS) 981 standard gave mean $^{206}Pb/^{204}Pb$, $^{207}Pb/^{204}Pb$, and $^{208}Pb/^{204}Pb$ ratios of 16.942066 ± 0.001295 (2SE), 15.500117 ± 0.001365 (2SE), and 36.725946 ± 0.003413 (2SE), respectively. These values agree within error with the values reported in Thirlwall

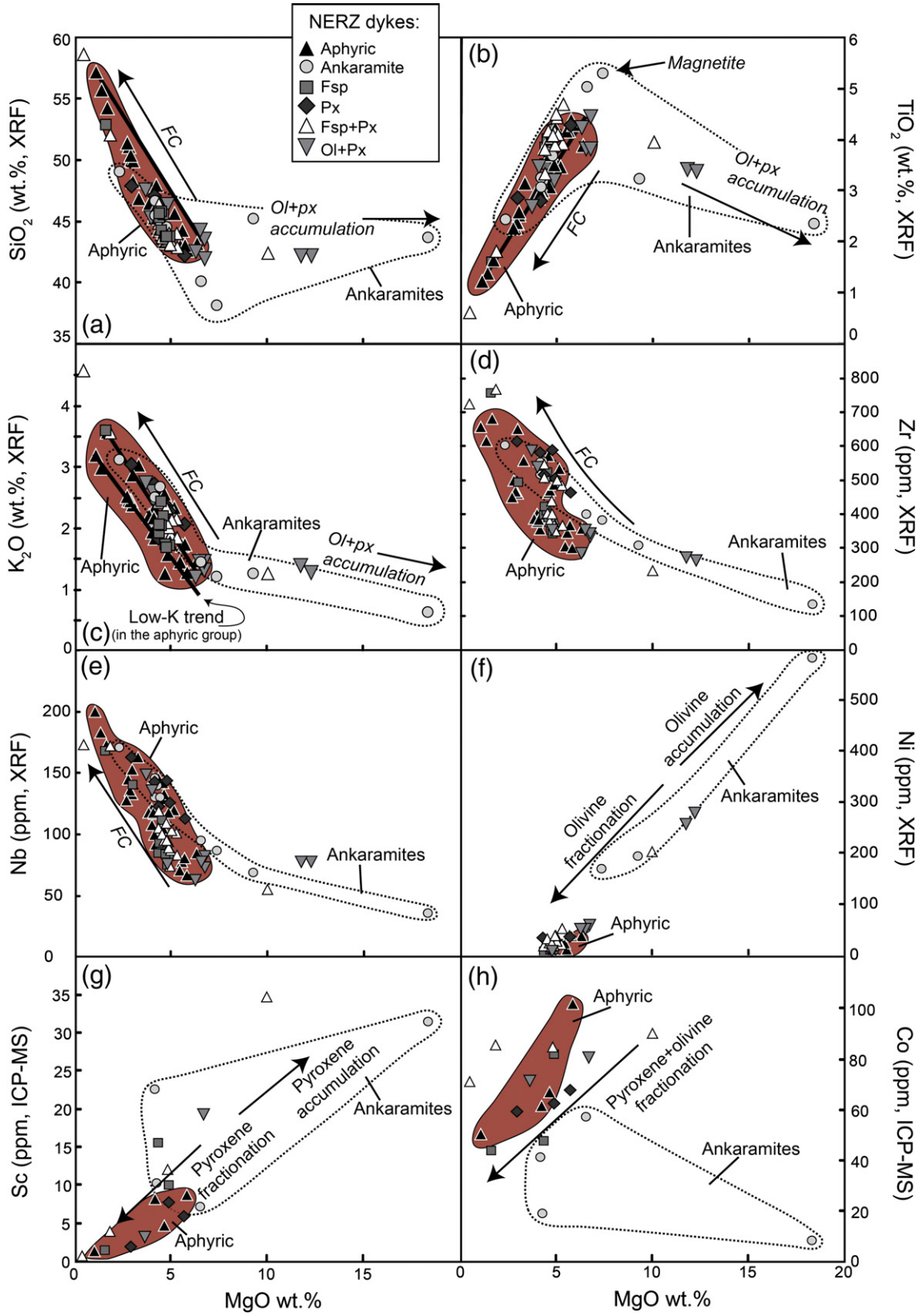

Fig. 4. Selected major and trace element variation diagrams for the NERZ dykes illustrating i) fractional crystallisation trends and ii) the effect of pyroxene and olivine accumulation in the crystal-rich ankaramite group. Aphyric samples, whose composition is unaffected by accumulation of phenocrysts are highlighted in red. Solid black lines represent fractional crystallisation models and are discussed in the text. FC = fractional crystallisation, px = pyroxene, ol = olivine. (For interpretation of the references to colour in this figure legend, the reader is referred to the web version of this article.)

(2002). Repeated analyses ($n=7$) of the international geological reference standard BHVO-2 (procedural standard) gave mean $^{206}Pb/^{204}Pb$, $^{207}Pb/^{204}Pb$, and $^{208}Pb/^{204}Pb$ ratios of 18.63399 ± 0.02207 (2SE), 15.54146 ± 0.00299 (2SE), and 38.23885 ± 0.02025 (2SE), respectively. These values agree within error with the values reported in Weis et al. (2006). Standard analyses are given in Tables S4–5. Both Nd and Pb blanks were less than 10 ppb which is negligible compared to the 400 ppb (Pb) to 800 ppb (Nd) measuring solutions used and hence no blank corrections were applied.

5. Results

5.1. Major and trace elements

Major and trace element data are reported in Table 1 for dykes with corresponding isotope analyses. The full data set is provided in Table S6, and variation diagrams are shown in Fig. S1 and Fig. 4. Trace elements and radiogenic isotope data are reported in Table 2. The dykes can be classified as silica-undersaturated foidite through basanite to trachyte on a

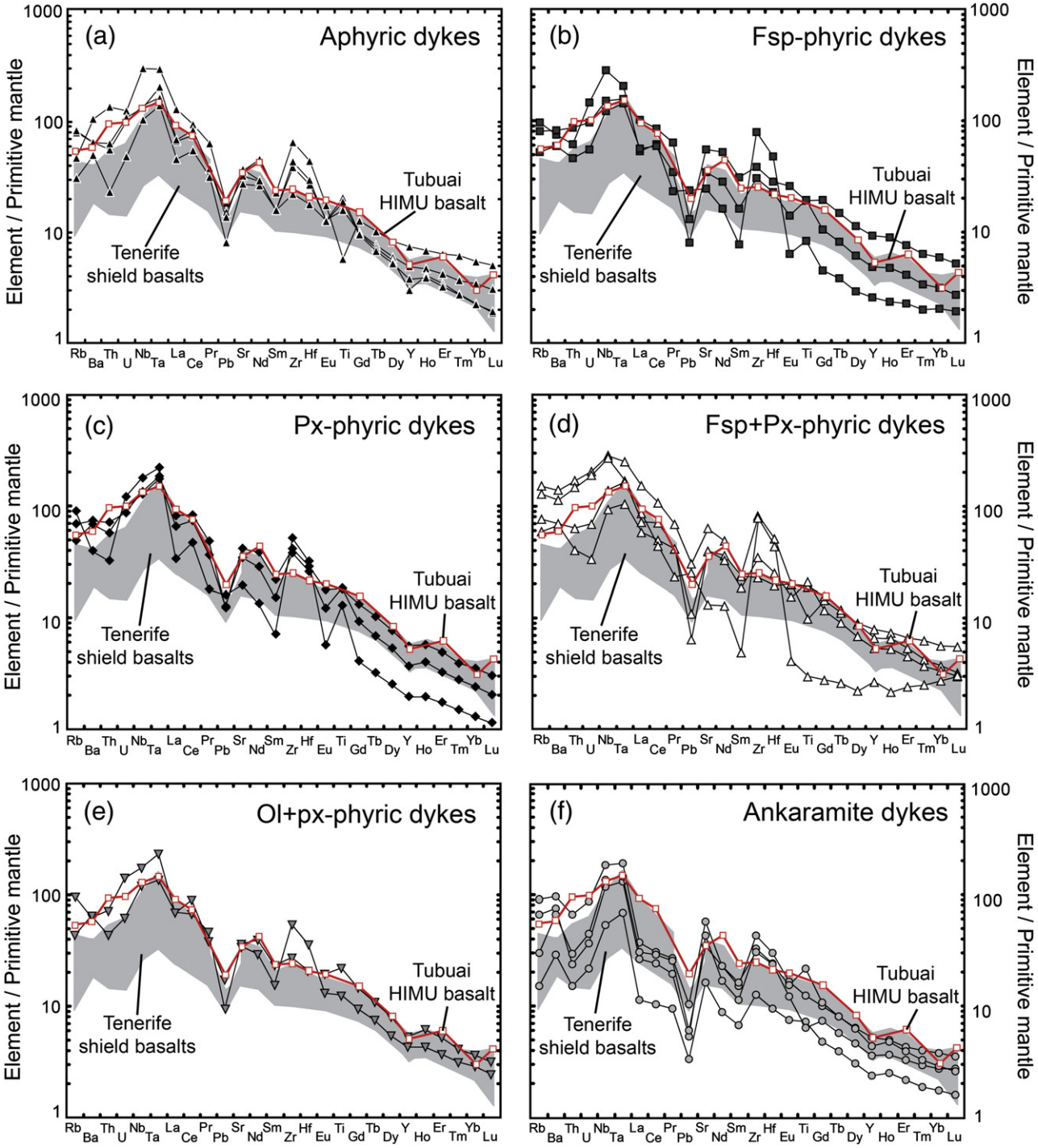

Fig. 5. Multi-element variation diagrams for dykes of the NERZ normalised to primitive mantle (Sun and McDonough, 1989). White square symbols are average Tubuai (HIMU) basalt shown for reference. Tubuai basalt data is taken from Chauvel et al. (1992) and normalised to primitive mantle. Shaded area shows the range for the shield basalts on Tenerife after Gurenko et al. (2006). All NERZ data shown were obtained by ICP-MS. Where duplicate ICP-MS analyses were performed, the average was plotted.

total alkali versus silica (TAS) plot (Fig. 3), with most of the dykes plotting in the basanite field. Only two ankaramite samples plot as foidites, one ankaramite plots as a picro-basalt, and one fsp + px-rich sample plots as a trachyte. Phono-tephrites to tephri-phonolites are similarly few. Several aphyric samples form a slightly less alkaline trend from trachy-basalt to trachy-andesite. This lower alkalinity closely resembles the shield basalt massifs on Tenerife (Fig. 3; Thirlwall et al., 2000). The tendency for most of the NERZ dykes to form a highly alkaline trend from basanite to tephri-phonolite, however, is similar to the trend displayed by the Las Cañadas and the younger Teide–Pico Viejo series (Fig. 3; Ablay et al., 1998; Neumann et al., 1999; Wiesmaier et al., 2011, 2012).

The dykes of the NERZ display a wide range in MgO content, from 0.5 to 18 wt.% (Fig. 4). The majority of the dykes have MgO<6.3 wt.%, with only ten, crystal-rich samples exceeding this value. The ankaramites, ol + px, and fsp + px dykes display the greatest major element variability of all the groups. The aphyric, fsp, and px groups, on the other hand, tend to form narrow linear trends on variation diagrams for most of the major elements. These latter groups demonstrate broadly increasing SiO_2, Al_2O_3, Na_2O, and K_2O and decreasing TiO_2, Fe_2O_3, and CaO with decreasing MgO, and a kinked trend for P_2O_5. The aphyric samples also demonstrate a split K_2O trend, with several samples showing lower K_2O at a given MgO content than the other petrographic groups (see Fig. 4c).

Selected trace element variations in the dykes are shown in Fig. 4 (with further diagrams provided in Fig. S2). The dykes show negative correlations between MgO and Rb, Sr, and Ba and very good co-linearity on a Zr–Nb plot (Fig. S3). Nickel contents are generally low (<100 ppm) except for some crystal-rich samples (ankaramites, two ol + px, one fsp + px), which have a maximum Ni content of 582 ppm. The compatible elements Ni, Co, and Sc all display marked trends to lower concentrations with decreasing MgO (Fig. 4).

Primitive mantle-normalised trace element patterns for the NERZ dykes are shown in Fig. 5. The dykes exhibit a broadly similar pattern to the Tenerife shield stage basalts given in Gurenko et al. (2006), showing enrichment in the light rare earth elements (LREE) relative to the heavy rare earth elements (HREE), a maximum at Nb–Ta, and a significant negative Pb anomaly, which are frequently observed for HIMU-derived lavas. The dykes are enriched in the large ion lithophile elements (LILE) and also in some of the high field strength elements (HFSE). Some groups also show severely depleted heavy rare earth element (HREE) patterns (Fig. 5b, c, d, f), which are discussed further on.

Table 3
Oxygen isotope and H_2O wt.% data for the NERZ whole rocks and crystal separates.

Sample	$\delta^{18}O$ ‰ (wr)	$\delta^{18}O$ ‰ (px)	$\delta^{18}O$ ‰ (ol)	H_2O wt.% (wr)	Petrographic group
NER-2	7.1			0.95	fsp
NER-3	6.2	5.1		0.43	ol + px
NER-10	5.7			0.39	fsp + px
NER-12	7.7			0.48	fsp
NER-13	6.4			0.65	fsp
NER-18A	7.0			0.59	fsp + px
NER-29	6.6			0.88	Aphyric
NER-37A	6.5			0.69	ol + px
NER-37W	7.0	4.9		1.16	Ankara
NER-40	8.4	4.8		1.90	px
NER-46	6.2			0.55	fsp + px
NER-47	6.6			0.92	Ankara
NER-57A	7.9			0.89	Ankara
NER-61	6.0			0.44	Aphyric
NER-65	7.2			0.63	fsp
NER-66	7.3			0.44	fsp + px
NER-70	6.7	5.9		0.86	px
NER-70A	6.4			0.65	px
NER-73	6.2			0.72	Aphyric
NER-77	6.2	5.3	5.6	0.54	Ankara
NER-81	6.4	4.7	4.6	1.33	ol + px
G2-D11	6.9			1.03	fsp
G2-D19	6.4			1.43	fsp + px
G2-D20	7.1			0.89	Aphyric
G2-D29	6.7			0.88	Aphyric
LC-7	7.6			1.27	fsp + px
LO-25	7.1			0.77	Aphyric

Samples are denoted with either "wr" (whole rock), "px" (pyroxene), or "ol" (olivine). See text for more details about the petrographic groupings of dykes.

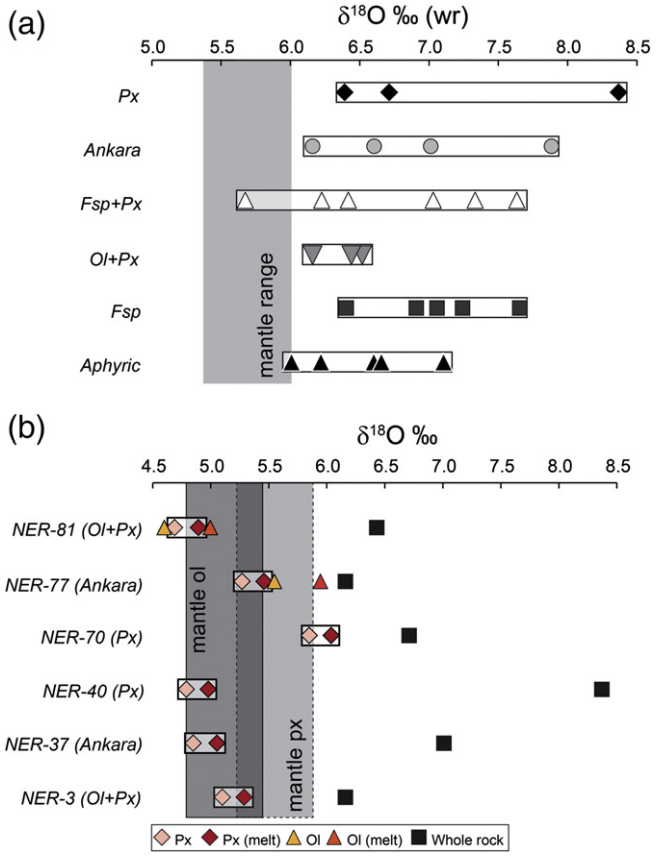

Fig. 6. a: Range of $\delta^{18}O$ values in the NERZ dykes relative to mantle values. b: Oxygen isotope values of NERZ phenocrysts, their estimated melt values, and the corresponding whole rock value. The following fractionation factors were used: $\Delta_{melt\text{-}ol} = 0.4‰$ (Eiler et al., 2000) and $\Delta_{melt\text{-}cpx} = 0.2‰$ (Gurenko et al., 2001). Pyroxene mineral-melt pairs are highlighted with rectangles. Note that all estimated $\delta^{18}O$ values are systematically lower than the measured wholerock (wr). The range in $\delta^{18}O$ values for mantle olivine and pyroxene is taken from Mattey et al. (1994).

5.2. O–Sr–Nd–Pb isotopes

Oxygen isotope data for whole rock and crystal separates are reported in Table 3 and plotted in Figs. 6 and 7 (and Fig. S4), and Sr–Nd–Pb isotope data are reported in Table 2 and plotted in Figs. 7–11 (and Figs. S5–6). The rift zone whole rocks display wide variation in $\delta^{18}O$ values (5.7–8.4‰) in contrast to relatively narrow ranges in $^{87}Sr/^{86}Sr$ (0.703077–0.703205), $^{143}Nd/^{144}Nd$ (0.51280–0.51297), $^{207}Pb/^{204}Pb$ (15.603–15.635), and $^{208}Pb/^{204}Pb$ (39.415–39.712). The range observed in $^{206}Pb/^{204}Pb$, although still narrow, varies slightly more than the other isotopes of Pb (19.591–19.838). Strontium ratios of the dykes fall into a narrow range within the previously reported fields for Tenerife lavas, while, on the other hand, the Nd ratios of the dykes form an almost vertical trend in Sr–Nd isotope space and span the entire range previously reported for Tenerife (Simonsen et al., 2000; Gurenko et al., 2006; Wiesmaier, 2010; Wiesmaier et al., 2011, 2012). In detail, some of the dykes trend towards elevated Sr isotope ratios with only minor or negligible variation in Nd ratios. Strontium and O isotopes correlate only weakly, with all of the samples with $^{87}Sr/^{86}Sr$ equal or greater than 0.70311 displaying elevated $\delta^{18}O$ values in the range 6.2–8.4‰. Lead isotopes plot in the field of

previously reported data for Tenerife. The NERZ dykes tend to be more radiogenic than the underlying Anaga shield massif but have overlapping compositions with the Central Shield (Roque del Conde) (Fig. 9). The transitional to evolved NERZ dykes (based on the TAS classification, Fig. 3) tend to cluster with respect to their lead isotopes and plot close to the field for transitional to evolved lavas erupted in the recent Teide–Pico Viejo complex (Wiesmaier et al., 2012).

Paleomagnetic data are available for some of the dykes analysed here (Delcamp et al., 2010, see Table S1). With respect to their Pb isotopes (Fig. 11), dykes identified as being older than 780 ka, i.e., galerías samples and those with reverse polarities ($n=10$), are well spread out in the dataset.

6. Discussion

6.1. Fractional crystallisation and crystal accumulation

Major element variation diagrams for the NERZ dykes display linear trends and kinks that are characteristic of fractional crystallisation of an assemblage including olivine, clinopyroxene, plagioclase, Fe–Ti oxides, and apatite (Fig. 4a to c and see Fig. S1). Broadly increasing Al_2O_3, Na_2O, and K_2O and decreasing Fe_2O_3 and CaO with decreasing MgO are indicative of olivine and pyroxene removal. The kink in the TiO_2 trend with increasing degree of differentiation suggests the onset of magnetite fractionation, which has previously been identified as the major Fe–Ti oxide phase in the dykes (Delcamp et al., 2010; Fig. 4b). A kink in the P_2O_5 trend indicates the onset of apatite fractionation. It is interesting to note split K_2O and Rb trends, which are observed only for the aphyric samples (Fig. 4c). These may reflect different crystallisation conditions for different pulses of dykes or a Rb-bearing mineral phase.

Trace element variations in the dykes are furthermore consistent with fractional crystallisation and incompatible behaviour of, e.g., Rb, Sr, Ba, Nb, and Zr (e.g. Fig. 4d, e and Fig. S2). Decreasing Sc and Ni with decreasing MgO is the result of crystallisation of pyroxene and olivine, respectively, whereas Co, which is compatible in both minerals, decreases only weakly with decreasing MgO (Fig. 4f to h). Many of the dyke samples show good positive correlation between Nb and Zr, as expected for a suite formed by fractional crystallisation (Fig. S3). Some samples, particularly aphyric types, plot at higher Nb concentrations. However, many of the samples that show high Nb/Zr also fall on the low K_2O trend. This may again be attributed to variations in crystallisation conditions, probably during multi-stage ascent of the rift zone magmas to the surface, as has been reported for the Canary Islands (cf. Hansteen et al., 1998; Stroncik et al., 2009). A low-K, high-Nb liquid can be produced by removal of a K-bearing phase in which Nb is incompatible, and Zr is at least moderately compatible, such as feldspar (see below).

We modelled fractional crystallisation by applying least squares minimisation only to the aphyric samples because i) the elemental trends displayed by most of the petrographic groups are mimicked by the aphyric group, and ii) the aphyric group more reliably represents liquid compositions than the porphyritic samples. The trends in the data can be explained by 27% fractional crystallisation of plagioclase, clinopyroxene, Fe–Ti oxides, olivine, and apatite in the proportions 41:25:18:11:5, respectively. Amphibole was not included in the model as it occurs only as a minor phase. Apatite, on the other hand, while also a minor phase, was included in the model as it exerts a major control on P_2O_5. This fractional crystallisation model can account for the lower K_2O trend in the aphyric group, but crystallisation of the same assemblage in the respective proportions 38:28:19:10:5 is required to explain the higher K_2O series. It would seem that the slightly lower K_2O trend can be explained by minor removal of plagioclase, and perhaps minor amphibole. All samples with MgO > 6.35 wt.% are exclusively porphyritic and belong to the ankaramite, ol + px, and fsp + px petrographic groups. These samples tend not to follow simple fractional crystallisation trends, and their major element scatter probably reflects crystal accumulation rather than liquid compositions (see Fig. 4). These relatively high MgO samples may be explained by various degrees of accumulation of olivine and clinopyroxene phenocrysts which would drive the composition of these samples to decreasing TiO_2, Al_2O_3, Fe_2O_3, Na_2O, and K_2O, constant or weakly increasing CaO, and fairly constant SiO_2 with increasing MgO (cf. Barker et al., 2009) (see arrows in Fig. 4).

6.2. Interaction between magma and island edifice

We use the volatile content of the samples as an indication of the degree of alteration before assessing isotopic variability due to magmatic processes. This is assuming that alteration will lead to elevated H_2O contents, but bearing in mind that low-temperature mineral precipitation from, e.g. groundwater, would have relatively high $\delta^{18}O$ values but low to minimal water content. Carbon dioxide contents are generally very low in the NERZ suite (<0.08% for all samples, except those taken in Galerías, which range from 0.04 to 3.12%). Water contents are also generally low, with most samples containing less than 1 wt.% water (58 out of 83 samples, with an average H_2O content of 0.63 wt.% among the subset of 58 samples). Samples with H_2O in excess of 2 wt.% ($n=2$) were not analysed for REE or isotopes. On primitive-mantle normalised trace element plots (Fig. 5), many of the dykes show enrichment in several of the LILE (e.g. Rb, Ba, Sr, and Ce) and HFSE (e.g. Zr, Hf, Th, and U). This trace element enrichment probably reflects diffuse, low temperature alteration, but this same process does not affect the HREE in the same way (Jochum and Verma, 1996). The depleted HREE patterns in Fig. 5 can therefore be used to provide insight into the nature of the source, as discussed later.

Many of the dykes have $\delta^{18}O$ values significantly higher than the mantle range ($5.7 \pm 0.3‰$; Ito et al., 1987; Harmon and Hoefs, 1995; Fig. 6). High $\delta^{18}O$ values coupled with high H_2O contents in a small number of samples ($n=3$, samples: NER-40, NER-57, and LC-7) strongly suggest that they have undergone low-temperature exchange of oxygen through interaction with meteoric water at $T \leq 150$ °C (e.g. Donoghue et al., 2008, 2010 and references therein) (Fig. 7a). Several samples, however, display elevated $\delta^{18}O$ values and relatively low H_2O contents (i.e. <0.9 wt.%, see Fig. 7a). This suggests that the oxygen isotope ratios of at least some of the samples reflect magmatic processes such as late-stage crustal interaction (discussed below) and/or that H_2O is not a reliable proxy for alteration.

Low temperature alteration appears not to have a significant effect on the radiogenic isotope systems as evidenced by the narrow ranges of ratios reported. Moreover, the dykes most prone to alteration (ankaramites) were leached prior to radiogenic isotope analysis to minimise any traces of altered material. By and large, Nd and Pb isotopes are regarded as being unaffected by post-eruptive hydrothermal alteration (Cousens et al., 1993) and hence they are interpreted to reliably reflect magmatic processes in the NERZ dykes.

Despite the observation that crustal assimilation in ocean island settings may be difficult to detect because of the compositional similarities between magma and assimilant (e.g. Taylor and Sheppard, 1986; O'Hara, 1998; Wolff et al., 2000; Wiesmaier, 2010), it is becoming increasingly recognised that ocean island magmas are susceptible to contamination by various components of the ocean crust and island edifice (e.g. Clague et al., 1995; Bohrson and Reid, 1997; Garcia et al., 1998; Kent et al., 1999; Harris et al., 2000; Wolff et al., 2000; Gurenko et al., 2001; Troll and Schmincke, 2002; Hansteen and Troll, 2003; Gaffney et al., 2005; Legendre et al., 2005; Aparicio et al., 2006; 2010; Troll et al., 2012; Wiesmaier et al., 2012). Potential assimilants include pre-island sediments and igneous ocean crust, plutonic rocks of the island core, and variably altered erupted materials that span a wide range in composition, particularly on Tenerife where there exist substantial volumes of felsic products in the volcanic pile (e.g. Wolff et al., 2000; Wiesmaier et al., 2012). Minor variations in O–Sr and Sr–Nd isotopes for the NERZ dykes are consistent with contamination by

hydrothermally altered edifice rocks, sediments, and/or altered ocean crust. These samples are discussed below and are not considered in the discussion of mantle source characteristics (in particular NER-37W, NER-47, NER-57, NER-77, LC-7, and G2-D20).

6.2.1. Oxygen isotope evidence for contamination

Oxygen isotope variations in the dykes suggest that while some of the samples have been affected by diffuse low temperature alteration, others potentially record contamination by material that has itself been hydrothermally altered. Many dyke samples have whole rock $\delta^{18}O$ values that are elevated relative to the mantle range, despite low H_2O contents in some of the samples (Fig. 7a). The $\delta^{18}O$ range in the dykes cannot be explained purely by fractional crystallisation, as this would only cause an increase in the $\delta^{18}O$ values of a rock suite of less than 1‰ (see the Rayleigh fractionation curve in Fig. 7; Sheppard and Harris, 1985; Bindeman, 2008). Laser fluorination oxygen isotope analysis of olivine and pyroxene mineral separates demonstrates that the phenocrysts systematically record lower $\delta^{18}O$ values than the corresponding bulk rock (see Fig. 6b; Table 3). Magma $\delta^{18}O$ values were estimated for the crystals using mineral-melt fractionation factors of $\Delta_{melt\text{-}ol} = 0.4‰$ (Eiler et al., 2000) and $\Delta_{melt\text{-}cpx} = 0.2‰$ (Gurenko et al., 2001). All estimated magma $\delta^{18}O$ values are lower than the measured whole rock. The high $\delta^{18}O$ values of the whole rocks must therefore be caused either by post-crystallisation groundmass alteration or, more plausibly, by late-stage contamination after formation of the phenocryst assemblage. In the context of the Sr–O isotope data (Fig. 7b, c), we suggest that

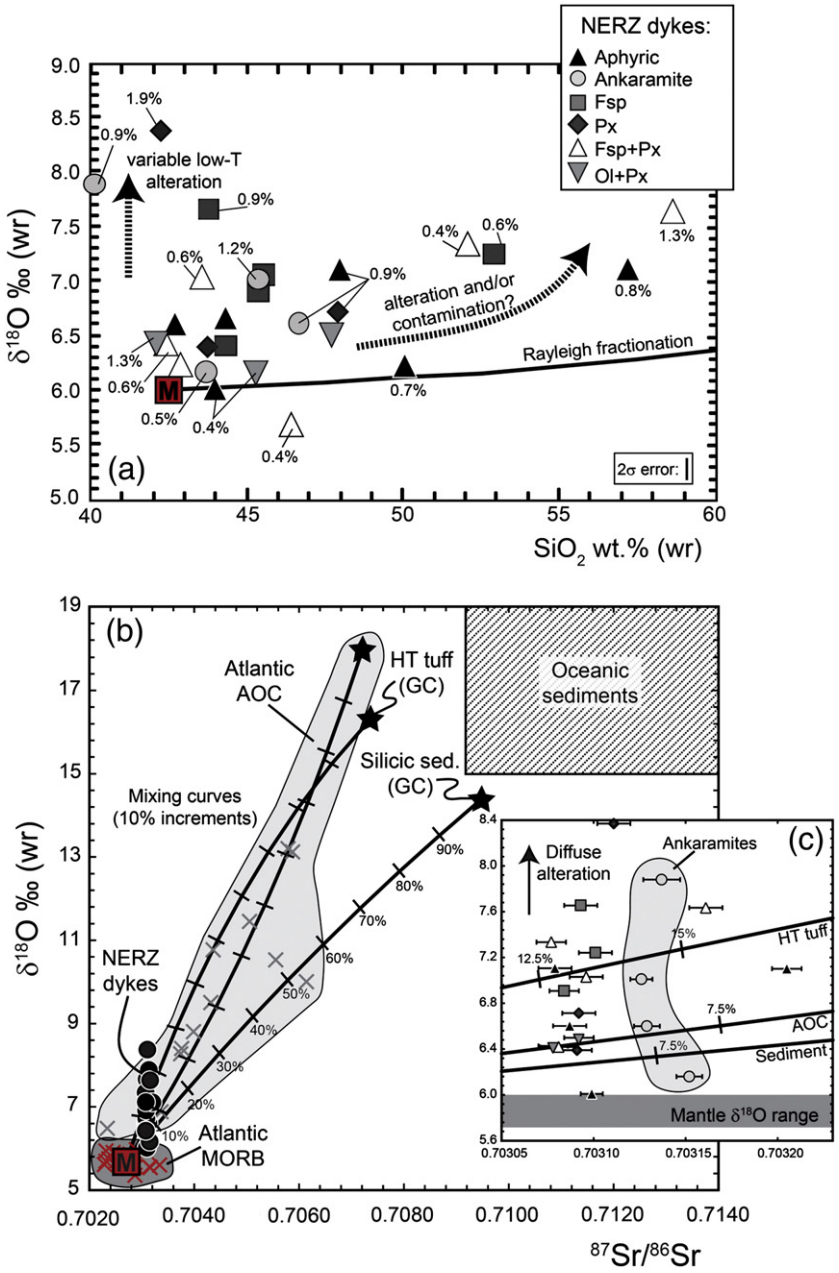

Fig. 7. a. $\delta^{18}O$ value versus SiO_2 wt.% for the NERZ dykes (wr = whole rock). Most of the dykes exhibit large and variable deviation from the trend expected for a magmatic suite related by fractional crystallisation (Rayleigh fractionation from a mantle parent, "M"). Values (in %) beside samples are H_2O contents. b and c: $\delta^{18}O$ value versus $^{87}Sr/^{86}Sr$ for the NERZ dykes. A series of mixing models are shown to illustrate that some of the $\delta^{18}O$ and $^{87}Sr/^{86}Sr$ variability in the dykes can be explained by mixing between a parental mantle source ("M") and i) minor amounts of hydrothermally ("HT") altered edifice rock (modelled using a tuff from Gran Canaria "GC", HAFT-3, with data from Troll, 2001; Troll and Schmincke, 2002), ii) ocean sediment (modelled using a siliciclastic xenolith from Gran Canaria, HAT-917C, with data from Troll, 2001; Hansteen and Troll, 2003), and/or iii) altered ocean crust ("AOC", data from Smith et al., 1995; Staudigel et al., 1995).

magmas with high $\delta^{18}O$ and relatively low H_2O contents ($\leq$1 wt.%) have assimilated minor amounts of crustal material. In terms of the timing of contamination, the discrepancy between the phenocryst and whole rock data can be explained as a result of the contaminant being isotopically recorded by the groundmass first, before becoming incorporated into the growing crystals (e.g. Duffield and Ruiz, 1998).

Potential contaminants include the upper sections of the igneous ocean crust that has undergone low temperature alteration (AOC), low temperature altered island edifice material, and ocean sediments, all of which would have relatively high $\delta^{18}O$ values. The oxygen isotope composition of altered igneous ocean crust is highly variable, and depends on the temperature and intensity of alteration. An average $\delta^{18}O$ value for the ocean crust of 9.96‰ is given by Staudigel et al. (1995), and a range of values from 4.1 to 8.6‰ for layer 2 of the Canary ocean crust is given in Hansteen and Troll (2003). An indication of the range of $\delta^{18}O$ in altered island edifice rocks comes from studies on Gran Canaria. Cousens et al. (1993) give a $\delta^{18}O$ range of 6.5 to 15.0‰ in altered ignimbrite matrices, Hansteen and Troll (2003) report a $\delta^{18}O$ range of 4.3 to 6.9‰ for core complex fragments, and Troll and Schmincke (2002) report a value of 16.2‰ for a hydrothermally altered tuff. Ocean sediments also display wide variation in $\delta^{18}O$ values, with a range of 11.5 to 28.5‰ given in Savin and Epstein (1969), and a range of 14.1 to 16.4‰ is given in Hansteen and Troll (2003) for quartz-rich sedimentary xenoliths from Gran Canaria. Small degrees of mixing (up to ~15%) between the NERZ dykes and a combination of such available crustal material can explain some of the variability in the oxygen isotope data (Fig. 7c).

Assimilation of ocean sediments and/or hydrothermally altered ocean crust and island edifice has been demonstrated for many of the Canary Islands, showing that late-stage modification of the primary composition of Canary magmas is common. For instance, Gurenko et al. (2001) found that variations in $\delta^{18}O$ and $\delta^{34}S$ in clinopyroxene-hosted melt inclusions from Gran Canaria can be most easily explained by up to 10% contamination by a mixture of ocean sediments and altered oceanic crust plus anhydrite. Thirlwall et al. (1997), Troll and Schmincke (2002), and Hansteen and Troll (2003) also discuss sediment assimilation in Gran Canaria magma genesis and the El Hierro eruption in 2011/12 likely represents another example of this phenomenon (Troll et al., 2012). Further, subaerial basalts on La Palma are thought to have undergone a small amount of assimilation (<2%) of low temperature altered material (pillow rinds) based on their elevated $^{187}Os/^{186}Os$ composition (Marcantonio et al., 1995). Assimilation of siliclastic and calc-silicate sediments by Lanzarote basalts has been shown to have occurred by Aparicio et al. (2006, 2010). Shallow-level assimilation of the pre-existing, hydrothermally altered Teno shield volcanic complex on Tenerife has also been suggested based on Pb isotope data from the NW rift zone (Hamilton et al., 2005). Assimilation of hydrothermally altered edifice by ascending plume magmas has furthermore been postulated for Hawaiian lavas (Garcia et al., 1998; Gaffney et al., 2005; Wang and Eiler, 2008),Tristan da Cunha lavas (Harris et al., 2000), and Cape Verde lavas (Barker et al., 2012) suggesting that this process may not be uncommon in ocean island settings in general.

6.2.2. Strontium isotope evidence for contamination

On a $^{143}Nd/^{144}Nd$–$^{87}Sr/^{86}Sr$ diagram, the NERZ dykes define a narrow $^{87}Sr/^{86}Sr$ range and a comparatively large spread in $^{143}Nd/^{144}Nd$, encompassing the data arrays previously reported for Tenerife shield basalts (e.g. Simonsen et al., 2000; Gurenko et al., 2006), dorsal lavas (Simonsen et al., 2000), and the Teide–Pico Viejo complex (Wiesmaier et al., 2012) (Fig. 8a). In detail, however, the dykes show a weak tendency towards higher $^{87}Sr/^{86}Sr$ at a given $^{143}Nd/^{144}Nd$ (Fig. 8b). We explored the possibility that this variation could be due to minor degrees of crustal contamination by performing mass balance assimilation and fractional crystallisation calculations (AFC), using the equations of DePaolo (1981). In the model, we used the most MORB-like of our samples as an approximation of a parental melt and the following possible contaminants: i) average DSDP sediment from south of Gran Canaria (Hoernle et al., 1991), ii) low temperature hydrothermally altered tuff from Gran Canaria (Troll, 2001; Donoghue et al., 2008), iii) a theoretical hydrothermally altered felsic island edifice rock with slightly lower $^{143}Nd/^{144}Nd$ than the measured tuff from Gran Canaria, and iv) hydrothermally altered pumice from Tenerife (Palacz and Wolff, 1989). The end-members used in the AFC calculations are given in Table S7, and the results of the AFC models are plotted in Fig. 8b. We do not discuss assimilation of the ocean crust with respect to Sr–Nd isotopes, since the isotopic signature of altered ocean crust is too similar to the dykes to cause a major change in their Sr–Nd ratios. The crustal end-members used in the model are considered representative of the kind of material expected in the volcanic pile of a mature Canary Island volcano. Given that radiogenic isotope data for hydrothermally altered ocean island edifice rocks are scant in the literature, we suppose that the composition of, e.g., the hydrothermally altered tuff from Gran Canaria can be reasonably extended to Tenerife, especially since very similar rock types occur on both islands (Donoghue, 2010). Note that the dykes with elevated $^{87}Sr/^{86}Sr$ plot within the "interaction" space between mantle-derived melt and a mixture of crustal components in $\delta^{18}O$–$^{87}Sr/^{86}Sr$ mixing models too (Fig. 7). Assimilation of felsic, potentially altered, material has previously been suggested for Tenerife (e.g. Palacz and Wolff, 1989; Wolff et al., 2000; Wiesmaier et al., 2012) and this is unsurprising in the context of the NERZ, given that felsic erupted products are common on the rift, especially in connection with mass unloading events (Carracedo et al., 2011). This suggests that they constitute a significant proportion of the sub-volcanic pile into which the NERZ dykes were intruded.

It is worth noting that trace element ratios vary widely between the older, Miocene basalts and Pliocene series on Tenerife (Simonsen et al., 2000). An explanation for this has been put forward by Simonsen et al. (2000), involving some form of island recycling, whereby younger magmas assimilate pre-existing rocks with similar isotopic characteristics (cf. O'Hara, 1998). The assimilated island edifice material may, however, have highly fractionated trace element ratios. This would be particularly evident in the case of recycling of felsic intrusives (cf. Wolff and Palacz, 1989; Wolff et al., 2000; Wiesmaier et al., 2012), underscoring the significance of this process in ocean island magma petrogenesis.

6.2.3. Pb isotope evidence for contamination

Given that the Pb isotope compositions of the dykes are expected to be unaffected by low temperature alteration processes (Cousens et al., 1993; Gaffney et al., 2005), it follows that assimilation of a hydrothermally altered component will also have limited impact on Pb isotopes. To illustrate this, note that the hydrothermally altered tuff (star in Figs. 9c and 10c) and the altered pumice from Tenerife (Palacz and Wolff, 1989; Figs. 9c and 10c) have overlapping Pb isotope compositions with the dykes and so cannot be distinguished as a contaminant. We hence interpret most of the dykes as reflecting primary Pb isotope compositions.

The dykes show restricted ranges in their $^{206}Pb/^{204}Pb$, $^{207}Pb/^{204}Pb$, and $^{208}Pb/^{204}Pb$ ratios and cluster around or near the Northern Hemisphere Reference Line (NHRL; Hart, 1984) (Figs. 9–11). On close inspection of the $^{207}Pb/^{204}Pb$–$^{206}Pb/^{204}Pb$ variations in the dykes, it can be seen that two samples have elevated $^{207}Pb/^{204}Pb$, placing them above the NHRL (Fig. 9). One of these samples (G2-D20, aphyric) has a high $\delta^{18}O$ value of 7.1‰, coupled with a moderate H_2O content of 0.89 wt.%, which precludes it from discussion of mantle sources since its primary Pb isotopic signature may have been compromised by oceanic sediment contamination. This sample also overlaps on Pb isotope diagrams with the field for Cretaceous uplifted deep ocean sediments exposed on Fuerteventura, which represent the sedimentary material underlying the Canary Islands (e.g. Stillman et al., 1975; data field drawn using data provided in Table S8 and Wiesmaier et al., 2012; see Figs. 9 and

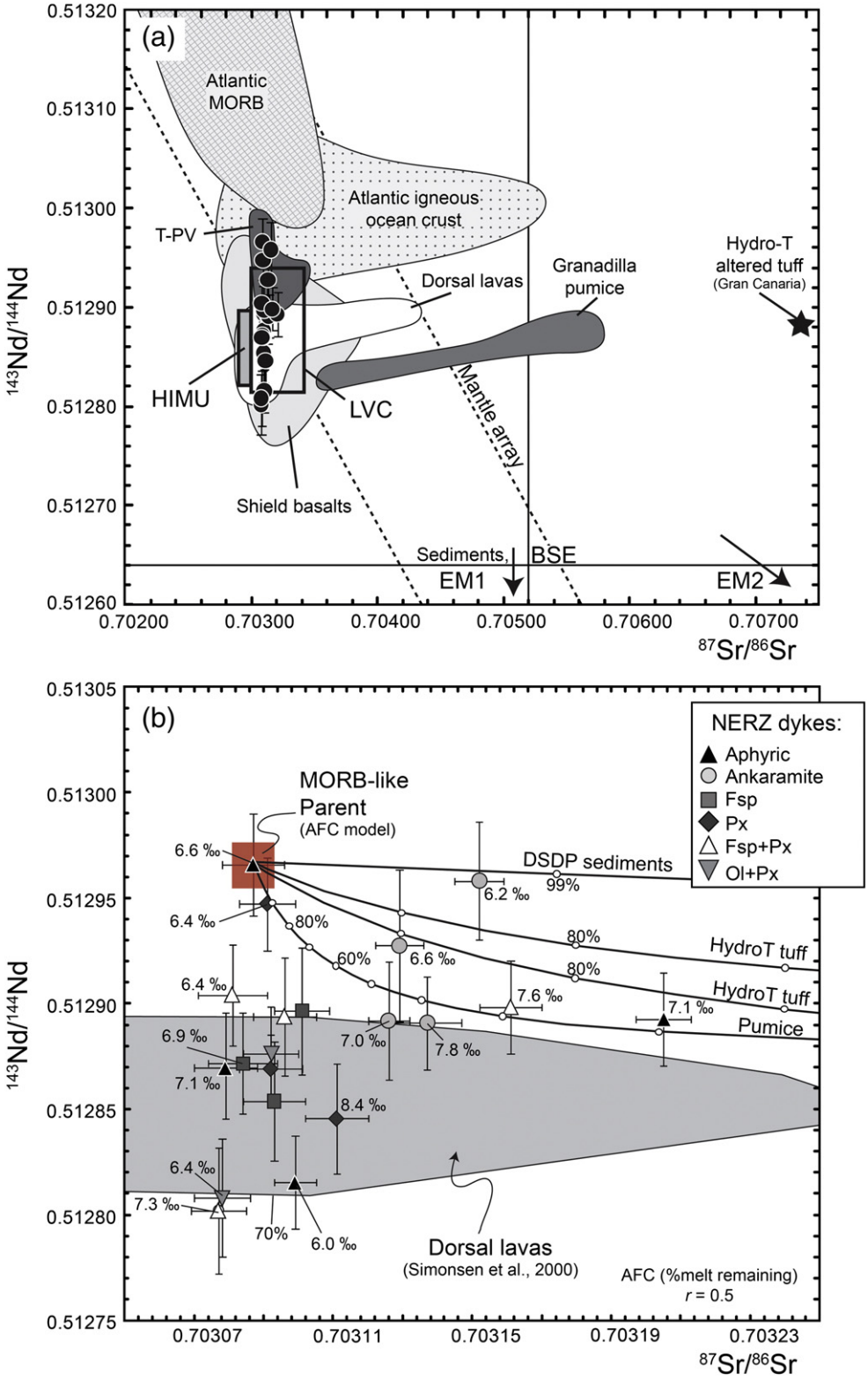

Fig. 8. Sr versus Nd isotope diagram for dykes of the NERZ. a: The rift zone dykes form a vertical array in Sr–Nd isotope space, spanning the values reported for Tenerife. Data sources: Atlantic MORB (Ito et al., 1987), Atlantic igneous ocean crust (Hoernle, 1998), shield basalts (Simonsen et al., 2000; Gurenko et al., 2006), dorsal lavas (Simonsen et al., 2000), Teide–Pico Viejo ("T–PV") lavas (Wiesmaier et al., 2012), hydrothermally altered tuff ("HydroT tuff"; Troll, 2001), and low velocity component ("LVC"; Hoernle et al., 1995). b: Detailed view of the Sr and Nd isotope variation within the NERZ dykes. Error bars are 2 standard deviations. Values (in ‰) given beside some samples are the corresponding $\delta^{18}O$ values. AFC models are discussed in the text.

10). The other sample plotting above the NHRL (NER-77, ankaramite) has a much larger $^{207}Pb/^{206}Pb$ error than the other NERZ samples, which extends below the NHRL. Given the large error on this sample, and the potential that it too has been contaminated by sediment based on its $^{87}Sr/^{86}Sr$ (Fig. 8), it is also omitted from subsequent discussion of mantle sources.

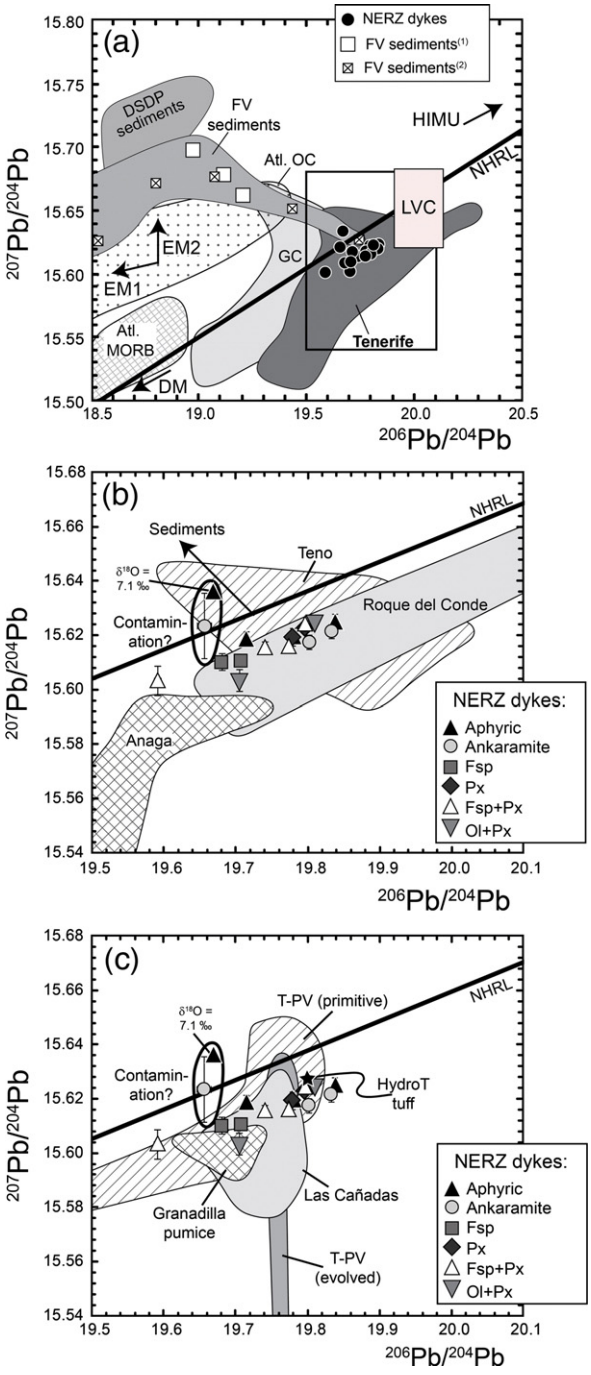

Fig. 9. $^{206}Pb/^{204}Pb$–$^{207}Pb/^{204}Pb$ isotope correlation diagrams for dykes of the North East Rift Zone (NERZ). Additional fields are drawn using data from Ito et al. (1987), Palacz and Wolff (1989), Hoernle et al. (1991), Hoernle et al. (1995), Thirlwall et al. (1997), Simonsen et al. (2000), and Gurenko et al. (2006). Sediment data from Fuerteventura Island ("FV") are shown for comparison using data given in Table S8 (1, open squares) and in Wiesmaier et al. (2012) (2, crossed squares). The Northern Hemisphere Reference Line ("NHRL") is drawn after Hart (1984). Mantle end-member compositions, indicated with arrows, are from Zindler and Hart (1986). Panels (b) and (c) are magnified from the box drawn on (a). The samples circled with a thick black line in panels (b) and (c) may be contaminated by sediments, based on their $\delta^{18}O$ values and their position above the NHRL (see text for discussion). The hydrothermally altered tuff from Gran Canaria ("HydroT tuff"; Troll, 2001) is shown with a black star on panel (c). Abbreviations: Atl. OC = Atlantic Ocean Crust; Atl. MORB = Atlantic Mid Ocean Ridge Basalt; DSDP = Deep Sea Drilling Program; GC = Gran Canaria; T–PV = Teide–Pico Viejo.

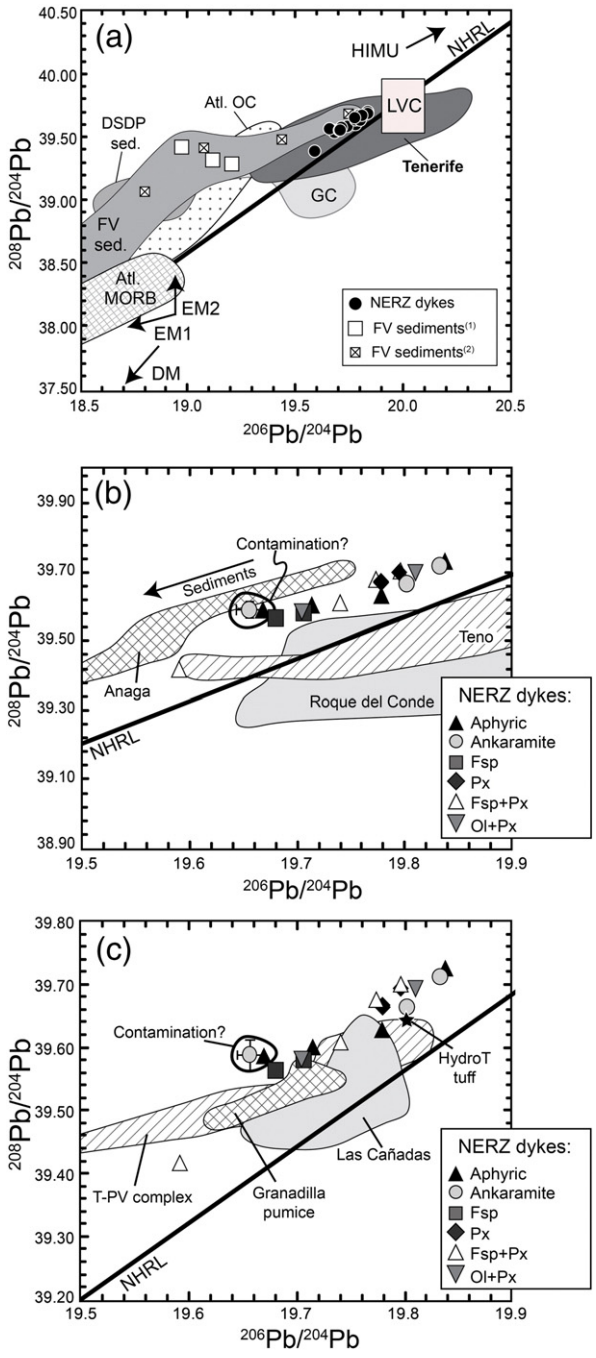

Fig. 10. $^{206}Pb/^{204}Pb$–$^{208}Pb/^{204}Pb$ isotope correlation diagrams for dykes of the North East Rift Zone (NERZ). The samples circled with a thick black line in panels (b) and (c) may be contaminated by sediments (see Fig. 9 and text for discussion). Data sources and abbreviations are given in the caption of Fig. 9.

6.3. A young HIMU signal for the rift

Although the primary O and Sr isotope signature of a number of NERZ dykes may be compromised by minor crustal contamination in combination with variable alteration, Nd and Pb isotopes are considered to be largely unaffected by interaction with meteoric or sea water (e.g. Cousens et al., 1993). Isotopes of Nd and Pb in the dykes are hence not expected to be significantly affected by contamination with hydrothermally altered material. Discarding the samples discussed above for Pb contamination, we interpret the remaining dykes to carry isotopic signatures representative of their mantle sources. In terms of $^{143}Nd/^{144}Nd$, the NERZ appears to be predominately derived from melting of a HIMU-like mantle component, with similar isotopic characteristics as described for the low velocity component (LVC) by Hoernle et al. (1995) (Fig. 8a). The LVC has been defined by Hoernle et al. (1995) as a common mantle source reservoir beneath the eastern Atlantic and

western and central Europe, with an isotope composition distinct from MORB. The involvement of a DMM component in the NERZ is also suggested by the $^{143}Nd/^{144}Nd$ systematics.

The NERZ dykes form a linear data array on Pb isotope plots (Figs. 9 and 10), indicating their derivation through mixing of two mantle components. On a $^{206}Pb/^{204}Pb$ versus $^{207}Pb/^{204}Pb$ plot, the dykes plot below the NHRL and extend from the LVC towards MORB-like (less radiogenic) compositions. This trend can be explained by the presence of young (less than 1.5 Ga) subducted crust in the source region, as has been shown by Thirlwall (1997). The data are hence consistent with derivation predominately from a young HIMU source, with admixture of a DMM component not unlikely (cf. Geldmacher and Hoernle, 2000, 2001; Simonsen et al., 2000; Gurenko et al., 2009). The data can also be considered to reflect involvement of an additional mantle component suggested to be common to many mantle plumes (e.g. the common or "C" component of Hanan and Graham, 1996). The "C" component is thought to originate from recycled, altered oceanic crust during the past 300 to 2000 Ma, giving rise to a $^{206}Pb/^{204}Pb$ range of 19.2 to 19.8 and a $^{207}Pb/^{204}Pb$ range of 15.55 to 15.65 (Hanan and Graham, 1996). However, the Pb isotope characteristics of the NERZ dykes can most simply be explained as arising from a substantial involvement of the young-HIMU component described by Thirlwall (1997), which has Pb isotope ratios similar to that of "C", and which is suggested to have itself given rise to mantle domains similar to the "C" component (Thirlwall, 1997). This explanation removes the need for substantial mantle mixing with respect to the NERZ, except for admixture of upper asthenosphere, and is consistent with other studies of mantle sources at Tenerife (e.g. Simonsen et al., 2000; Gurenko et al., 2006).

We note that an EM component appears to be either minimal or lacking in the NERZ. The involvement of an enriched component has been postulated for Tenerife, especially for the Anaga massif (Simonsen et al., 2000), but this does not appear to play an important role in the generation of the NERZ.

Trace element patterns are furthermore consistent with derivation of the NERZ magmas from a HIMU-like source (Fig. 5). The notable Pb minimum displayed by the NERZ dykes coupled with the wide range in Ce/Pb ratios (~25 to 74), that extend to anomalously high values in some dykes, may be attributed to subduction zone processing of ocean crust during the generation of a HIMU source, resulting in relative Pb depletion (e.g. Chauvel et al., 1992; Peucker-Ehrenbrink et al., 1994). However, Pb depletion may alternatively be a result of the melting environment (Thirlwall, 1997). Moreover, anomalously high Ce/Pb ratios (i.e. significantly exceeding the supposed average mantle value of 25) have been noted in clinopyroxene cumulate rocks from Tenerife and St. Helena (Thirlwall, 1997), which seems to be the most likely explanation for the porphyritic dykes from the NERZ, where crystal accumulation has been identified using major and trace element variations (Fig. 4). Conspicuously low HREE abundances in some dykes (e.g. Fig. 5b, c, d, and f) provide further insight to the nature of the source. Differences in the level of HREE enrichment among the dykes indicate that batches of magma were likely generated at varying depths of the melting column, or involved differing proportions of garnet in the source region, as has been discussed by Gurenko et al. (2006 and references therein).

6.3.1. Constraints on the spatial and temporal evolution of the mantle source

Of the three shield volcanoes on Tenerife, the $^{206}Pb/^{204}Pb$–$^{143}Nd/^{144}Nd$ and the $^{206}Pb/^{204}Pb$–$^{207}Pb/^{204}Pb$ compositions of the dykes appear to be most similar to the composition of the Roque del Conde massif (the Central Shield) (Figs. 9 and 10). This is consistent with the hypothesis put forward by Guillou et al. (2004) and Carracedo et al. (2011) that the Miocene–Pliocene NERZ initiated as an extension of the Central Shield that grew towards the Anaga massif in the NE of the island (Fig. 1b). The NERZ dykes also overlap with the Teno massif, but do not extend to the low $^{206}Pb/^{204}Pb$–$^{207}Pb/^{204}Pb$ values exhibited by the Anaga massif. We therefore suggest that, at least at its initiation, the NERZ had a separate mantle source and plumbing system to Anaga.

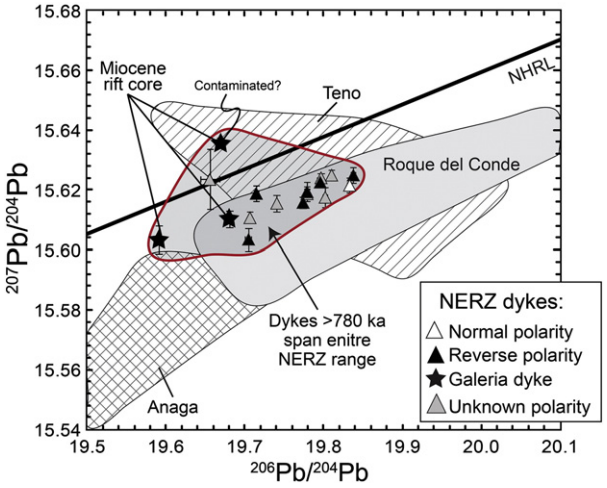

Fig. 11. $^{206}Pb/^{204}Pb$–$^{207}Pb/^{204}Pb$ isotope variation diagram for dykes of the North East Rift Zone (NERZ), with symbols corresponding to the ages of the dykes. Magnetic polarites are taken from Delcamp et al. (2010) and reported in Table S1: reverse polarity dykes are ≥780 ka old; normal polarity dyke is ≤780 ka old. Black stars are galerías samples, which probably represent the oldest, Miocene age, part of the rift (Carracedo et al., 2011).

Temporal constraints can be placed on our data using the magnetic polarities and $^{40}Ar/^{39}Ar$ ages obtained for dykes of the NERZ by Delcamp et al. (2010). Reversed polarity dykes are ≥780 ka old and normal polarity dykes are ≤780 ka old. In addition, the galerías samples can be taken as representative of the core of the rift, which may be as old as the Miocene (2.71 ± 0.06 Ma, Carracedo et al., 2011). Note, however, that the galerías samples did not give reliable magnetic polarity results due to dynamite shocking (Delcamp et al., 2010). We can hence infer that the Pb isotope systematics of the rift have been largely unchanging through its evolution, as the samples identified as being relatively old, i.e., galerías and reverse polarity dykes, span the entire $^{206}Pb/^{204}Pb$, $^{207}Pb/^{204}Pb$, and $^{208}Pb/^{204}Pb$ range of the NERZ dykes (Fig. 11). The dykes of unknown polarities are well spread out in the NERZ data array and are isotopically indistinguishable from the dated dykes.

Similarity between the $^{206}Pb/^{204}Pb$–$^{143}Nd/^{144}Nd$ and $^{206}Pb/^{204}Pb$–$^{207}Pb/^{204}Pb$ values of the younger Las Cañadas series and those of the NERZ are also evident and suggests that these systems also shared a similar parental magma source (Figs. 9c, S6). This seems plausible given that the Pleistocene NERZ evolved and erupted coeval to the Las Cañadas volcano (Carracedo et al., 2011). The $^{206}Pb/^{204}Pb$–$^{207}Pb/^{204}Pb$ for the younger (<200 ka) Teide–Pico Viejo complex (T–PV), on the other hand, overlaps with the NERZ but also extends to less radiogenic $^{206}Pb/^{204}Pb$ and $^{207}Pb/^{204}Pb$ than both the NERZ and Las Cañadas erupted products (Fig. 9c). The T–PV complex also plots to the higher end of the $^{143}Nd/^{144}Nd$ range displayed by the NERZ dykes. This observation, combined with the Pb isotope evidence, suggests slightly different source characteristics for this most recent phase of magmatism, which seems to reflect a greater DMM input. By and large, however, the source feeding the central part of the island seems to have persisted from the Central Shield building phase in the Miocene through to the evolution of the NERZ and the Las Cañadas edifice (Pliocene), and only underwent minor isotopic change at the time of, or just prior to, initiation of the T–PV magmatism.

The observations detailed above are less clear in terms of $^{206}Pb/^{204}Pb$–$^{208}Pb/^{204}Pb$. On a $^{206}Pb/^{204}Pb$–$^{208}Pb/^{204}Pb$ diagram, the dykes plot parallel to the NHRL and trend towards more radiogenic values

than the Anaga field (Fig. 10). This trend towards higher $^{206}Pb/^{204}Pb$–$^{208}Pb/^{204}Pb$ is mirrored by the Teno and Roque del Conde volcanoes (Fig. 10b). Some of the dykes also overlap with members of the Las Cañadas series on Tenerife on a $^{206}Pb/^{204}Pb$–$^{208}Pb/^{204}Pb$ diagram (Fig. 10c). This overlap, in turn, argues for a similar central source for the NERZ and the Las Cañadas volcano.

This almost persistent central source from the Miocene to Pliocene on Tenerife (Roque del Conde, Las Cañadas, NERZ) can be placed in the context of the "blob model" for Canary Island magmatism (Hoernle et al., 1991; Hoernle and Schmincke, 1993), wherein a deep narrow plume beneath the islands disperses into a zone of young HIMU-like mantle blobs entrained within DMM asthenospheric material. We suggest that a large, discrete column ("blob") of young HIMU-like mantle occupied the melting zone beneath central Tenerife from the Miocene to Pliocene. The spatial persistence of this "blob" was probably accommodated in part by the slow rate of plate motion beneath the Canaries (~10 mm yr^{-1}; Duncan, 1981; Morgan, 1983). The recent T–PV complex, in contrast, probably reflects a waning HIMU influence and greater incorporation of DMM material, possibly due to edge-entrainment of DMM into the blob, or thinning of the blob with time. Taking the onset of Central Shield magmatism at ca. 11.9 Ma (Guillou et al., 2004) and the youngest date obtained for the NERZ of 0.56 Ma (Delcamp et al., 2010), we obtain an estimated time span of ca. 11 Ma corresponding to the young HIMU contribution from this "blob". This time span is a maximum estimate, however, as it does not take into account the period of quiescence following the shield building stage when no HIMU-like magmatism occurred. According to the blob model of Hoernle and Schmincke (1993), pauses like this may reflect entrainment of cooler asthenosphere in the melting zone beneath an island, but we cannot speculate on this due to the lack of erupted or intruded material for this time span. Assuming a mantle upwelling rate of ca. 10 mm yr^{-1} (e.g. Iwamori et al., 1995; Ito et al., 1999; Barker et al., 2010), a maximum limit on the vertical extent of the blob can be determined to ca. 110 km. Although discrete mantle packages on this scale are accommodated in the blob model, they are most likely constrained to the centre of an upwelling "blob" (see figure 9 in Hoernle and Schmincke, 1993).

7. Summary of the NERZ petrogenesis

The NERZ on Tenerife presents an excellent opportunity to study the petrogenesis of a rapidly intruded volcanic rift. Dykes that intruded the rift zone display wide petrological variability, principally controlled by fractional crystallisation and crystal accumulation. These processes probably occurred at various depths during multi-stage ascent and stagnation in small, intermittent magma chambers (cf. Stroncik et al., 2009). Rift unloading events initially promoted ascent of mafic magma (Longpré et al., 2009; Carracedo et al., 2011), as disruption to the plumbing system and associated decompression would have facilitated magma migration from lower crustal and upper mantle depths leading to eruption of crystal-rich, dense magma types such as the ankaramite dyke group (cf. Longpré et al., 2009; Manconi et al., 2009).

Migration of rift zone magmas within the pre-existing volcanic edifice allowed for minor mid- to shallow level crustal assimilation of probably a mixture of hydrothermally altered components and ocean sediments (up to about 15% crustal input). This resulted in elevated $\delta^{18}O$ values and slightly perturbed $^{87}Sr/^{86}Sr$ values for some of the dykes. Recognition of these effects allows for identification of "compromised" samples, not useful in identifying the mantle sources feeding the rift. To this end, Nd and Pb isotopes are most insightful, and are not easily affected by low temperature hydrothermal processes (including assimilation of altered material). The principal source components in generating the rift zone magmas appear to be a young HIMU-like plume source that involved subducted crust with a residence time of less than 1.5 Ga, with admixture of upper depleted mantle (DMM) (Thirlwall, 1997; Simonsen et al., 2000; Gurenko et al., 2006). This is consistent with trace element patterns for the dykes and an enriched mantle component (EM) could not be identified for the rift.

Lead isotopes support the proposal that the NERZ initiated as an extension of the Central (Roque del Conde) Shield massif (cf. Guillou et al., 2004; Carracedo et al., 2011). The similar isotope systematics of the NERZ and the post-shield Las Cañadas series also suggest that these units co-evolved and shared a similar mantle source. These observations imply that the source feeding the central part of Tenerife has been isotopically almost constant from the Miocene Central Shield building phase through to the evolution of the NERZ and the Las Cañadas central edifice in the Pliocene. We also propose that the source for the recent Teide–Pico Viejo complex shows only minor isotopic differences to the preceding central magmatism on Tenerife, possibly reflecting the waning influence of the HIMU mantle "blob" that fed the island's central volcanoes since the Miocene. We thus suggest that a consistent "blob" of young HIMU mantle, $\leq$100 km in vertical extent, provided the source for the Central Shield, the NERZ, and the Las Cañadas magmatism and that the Teide–Pico Viejo complex possibly reflects entrainment of greater amounts of DMM with time.

Acknowledgements

We are grateful to F. Rawoot for technical support and oxygen analyses in Cape Town; B. van der Wagt for ICP-MS and MC-ICPMS analyses in Amsterdam; G. Davies, L. Font, R. Smeets, and M. Klaver for technical and laboratory support in Amsterdam; and D. Rau for XRF analyses at Geomar. M. Klaver is also thanked for analysing some of the samples by TIMS. L. Dallai, E.M. Jolis, F.M. Meade, K. Zaczek, and S. Wiesmaier are thanked for stimulating discussions. A. Gurenko, L. Dallai, and L. Reisberg are thanked for thoughtful reviews that helped to improve the manuscript. L. Reisberg is also thanked for editorial handling of the manuscript. This work was supported by a Science Foundation Ireland (SFI) grant to VRT and a Royal Swedish Academy of Sciences grant (KVA) to FMD.

Appendix A. Supplementary data

Supplementary data to this article can be found online at http://dx.doi.org/10.1016/j.chemgeo.2012.10.013.

References

Ablay, G.J., Carroll, M.R., Palmer, M.R., Marti, J., Sparks, R.S.J., 1998. Basanite–phonolite lineages of the Teide–Pico Viejo volcanic complex, Tenerife, Canary Islands. Journal of Petrology 39, 905–936.

Abratis, M., Schmincke, H.-U., Hansteen, T.H., 2002. Composition and evolution of submarine volcanic rocks from the central and western Canary Islands. International Journal of Earth Sciences (Geologische Rundschau) 91, 562–582.

Ancochea, E., Fuster, J.M., Ibarrola, E., Cendrero, A., Coello, J., Hernan, F., Cantagrel, J.M., Jamond, C., 1990. Volcanic evolution of the island of Tenerife (Canary Islands) in the light of new K–Ar data. Journal of Volcanology and Geothermal Research 44, 231–249.

Anguita, F., Hernán, F., 1975. A propagating fracture model versus a hot-spot origin for the Canary Islands. Earth and Planetary Science Letters 27, 11–19.

Anguita, F., Hernán, F., 2000. The Canary Islands origin: a unifying model. Journal of Volcanology and Geothermal Research 103, 1–26.

Aparicio, A., Bustillo, M.A., García, R., Araña, V., 2006. Metasedimentary xenoliths in the lavas of the Timanfaya eruption (1730–1736, Lanzarote, Canary Islands): metamorphism and contamination processes. Geological Magazine 143, 181–193.

Aparicio, A., Tassinari, C.C.G., García, R., Araña, V., 2010. Sr and Nd isotope composition of the metamorphic, sedimentary and ultramafic xenoliths of Lanzarote (Canary Islands): implications for magma sources. Journal of Volcanology and Geothermal Research 143–150.

Barker, A.K., Holm, P.M., Peate, D.W., Baker, J.A., 2009. Geochemical stratigraphy of submarine lavas (3–5 Ma) from the Flamengos Valley, Santiago, Southern Cape Verde Islands. Journal of Petrology 50, 169–193.

Barker, A.K., Holm, P.M., Peate, D.W., Baker, J.A., 2010. A 5 million year record of compositional variations in mantle sources to magmatism on Santiago, southern Cape Verde archipelago. Contributions to Mineralogy and Petrology 160, 133–154.

Barker, A.K., Troll, V.R., Ellam, R.M., Hansteen, T.H., Harris, C., Stillman, C.J., Andersson, A., 2012. Magmatic evolution of the Cadamosto Seamount, Cape Verde:

beyond the spatial extent of EM1. Contributions to Mineralogy and Petrology 163, 949–965.
Bindeman, I., 2008. Oxygen isotopes in mantle and crustal magmas as revealed by single crystal analysis. Reviews in Mineralogy and Geochemistry 69, 445–478.
Bohrson, W.A., Reid, M.R., 1997. Genesis of silicic peralkaline volcanic rocks in an ocean island setting by crustal melting and open system processes: Socorro Island, Mexico. Journal of Petrology 38, 1137–1166.
Carracedo, J.C., 1994. The Canary Islands: an example of structural control on the growth of large oceanic island volcanoes. Journal of Volcanology and Geothermal Research 60, 225–242.
Carracedo, J.C., 1999. Growth, structure, instability and collapse of Canarian volcanoes and comparisons with Hawaiian volcanoes. Journal of Volcanology and Geothermal Research 94, 1–19.
Carracedo, J.C., Day, S., Guillou, H., Rodríguez Badiola, E., Canas, J.A., Pérez Torrado, F.J., 1998. Hotspot volcanism close to a passive continental margin: the Canary Islands. Geological Magazine 135, 591–604.
Carracedo, J.C., Rodríguez Badiola, E., Guillou, H., Paterne, M., Scaillet, S., Pérez Torrado, F.J., Paris, R., Fra-Paleo, U., Hansen, A., 2007. Eruptive and structural history of Teide volcano and rift zones of Tenerife, Canary Islands. Geological Society of America Bulletin 19, 1027–1051. http://dx.doi.org/10.1130/B26087.1.
Carracedo, J.C., Guillou, H., Nomade, S., Rodríguez Badiola, E., Paris, R., Troll, V.R., Wiesmaier, S., Delcamp, A., Fernández-Turiel, J.L., 2011. Evolution of ocean-island rifts: the northeast rift zone of Tenerife, Canary Islands. Geological Society of America Bulletin 123, 562–584.
Chauvel, C., Hofmann, A.W., Vidal, P., 1992. HIMU-EM: the French Polynesian connection. Earth and Planetary Science Letters 110, 99–119.
Clague, D.A., Moore, J.G., Dixon, J.E., Friesen, W.B., 1995. Petrology of submarine lavas from Kilauea's Puna Ridge, Hawaii. Journal of Petrology 36, 299–349.
Cousens, B.L., Spera, F.J., Dobson, P.F., 1993. Post-eruptive alteration of silicic ignimbrites and lavas, Gran Canaria, Canary Islands: strontium, neodymium, lead, and oxygen isotopic evidence. Geochimica et Cosmochimica Acta 57, 631–640.
Davies, G.R., Stolz, A.J., Mahotkin, I.L., Nowell, G.M., Pearson, D.G., 2006. Trace element and Sr–Pb–Nd–Hf isotope evidence for ancient, fluid-dominated enrichment of the source of Aldan Shield lamproites. Journal of Petrology 47, 1119–1146.
Day, J.M.D., Pearson, G., Macpherson, C.G., Lowry, D., Carracedo, J.C.C., 2009. Pyroxenite-rich mantle formed by recycled oceanic lithosphere: oxygen–osmium isotope evidence from Canary Island lavas. Geology 37, 555–558.
Delcamp, A., Petronis, M.S., Troll, V.R., Carracedo, J.C., van Wyk de Vries, B., Perez-Torrado, F.J., 2010. Vertical axis rotation of the upper portions of the North-East rift of Tenerife Island inferred from paleomagnetic data. Tectonophysics 492, 40–59.
Delcamp, A., Troll, V.R., van Wyk de Vries, B., Carracedo, J.C., Petronis, M.S., Pérez-Torrado, F.J., Deegan, F.M., 2012. Dykes and structures of the NE-rift of Tenerife, Canary Islands: a record of stabilisation and destabilisation of ocean island rift-zones. Bulletin of Volcanology 74, 963–980.
Demény, A., Vennemann, T.W., Hegner, E., Ahijado, A., Casillas, R., Nagy, G., Homonnay, Z., Gutierrez, M., Szabó, Cs, 2004. H, O, Sr, Nd, and Pb isotopic evidence for recycled oceanic crust in the Transitional Volcanic Group of Fuerteventura, Canary Islands, Spain. Chemical Geology 205, 37–54.
DePaolo, D.J., 1981. Trace element and isotopic effects of combined wallrock assimilation and fractional crystallization. Earth and Planetary Science Letters 53, 189–202.
Donoghue, E., 2010. Fluid-rock interaction in the Tejeda caldera, Gran Canaria, and the Las Cañadas caldera, Tenerife (Canary Islands). PhD thesis. University of Dublin, Trinity College.
Donoghue, E., Troll, V.R., Harris, C., O'Halloran, A., Walter, T.R., Pérez Torrado, F.J., 2008. Low-temperature hydrothermal alteration of intra-caldera tuffs, Miocene Tejeda caldera, Gran Canaria, Canary Islands. Journal of Volcanology and Geothermal Research 176, 551–564.
Donoghue, E., Troll, V.R., Harris, C., 2010. Fluid–rock interaction in the Miocene, Post-Caldera, Tejeda intrusive complex, Gran Canaria (Canary Islands): insights from mineralogy, and O- and H-isotope geochemistry. Journal of Petrology 51, 2149–2176.
Duffield, W.A., Ruiz, J., 1998. A model that helps explain Sr-isotope disequilibrium between feldspar phenocrysts and melt in large-volume silicic magma systems. Journal of Volcanology and Geothermal Research 87, 7–13.
Duncan, R.A., 1981. Hotspots in the Southern Oceans — an absolute frame of reference for motion of the Gondwana continents. Tectonophysics 74, 29–42.
Edgar, C.J., Wolff, J.A., Nichols, H.J., Cas, R.A.F., Martí, J., 2002. A complex Quaternary ignimbrite-forming phonolitic eruption: the Poris Member of the Diego Hernández Formation (Tenerife, Canary Islands). Journal of Volcanology and Geothermal Research 118, 99–130.
Eggins, S.M., Woodhead, J.D., Kinsley, L.P.J., Mortimer, G.E., Sylvester, P., McCulloch, M.T., Hergt, J.M., Handler, M.R., 1997. A simple method for the precise determination of ≥40 trace elements in geological samples by ICPMS using enriched isotope internal standardisation. Chemical Geology 134, 311–326.
Eiler, J.M., Crawford, A., Elliott, T., Farley, K.A., Valley, J.W., Stolper, E.M., 2000. Oxygen isotope geochemistry of oceanic-arc lavas. Journal of Petrology 41, 229–256.
Elburg, M., Vroon, P., van der Wagt, B., Tchalikian, A., 2005. Sr and Pb isotopic composition of five USGS glasses (BHVO-2G, BIR-1G, TB-1G, NKT-1G). Chemical Geology 223, 196–207.
Fagereng, A., Harris, C., LaGrange, M., Stevens, G., 2008. Stable isotope study of the Archean rocks of the Vredefort impact structure, central Kaapvaal Craton, South Africa. Contributions to Mineralogy and Petrology 155, 63–78.
Gaffney, A.M., Nelson, B.K., Reisberg, L., Eiler, J., 2005. Oxygen-osmium isotope systematics of West Maui lavas: a record of shallow-level magmatic processes. Earth and Planetary Science Letters 239, 122–139.
Garcia, M.O., Ito, E., Eiler, J.M., Pietruszka, A.J., 1998. Crustal contamination of Kilauea volcano magmas revealed by oxygen isotope analyses of glass and olivine from Puu Oo eruption lavas. Journal of Petrology 39, 803–817.
Geldmacher, J., Hoernle, K., 2000. The 72 Ma geochemical evolution of the Madeira hotspot (eastern North Atlantic): recycling of Paleozoic (≤500 Ma) oceanic lithosphere. Earth and Planetary Science Letters 183, 73–92.
Geldmacher, J., Hoernle, K., 2001. Corrigendum to: 'the 72 Ma geochemical evolution of the Madeira hotspot (eastern North Atlantic): recycling of Paleozoic (≤500 Ma) oceanic lithosphere' [Earth Planet. Sci. Lett. 183 (2000) 73–92]. Earth and Planetary Science Letters 186, 333.
Geldmacher, J., Hoernle, K., Van den Bogaard, P., Zankl, G., Garbe-Schönberg, D., 2001. Earlier history of the ≥70-Ma-old Canary hotspot based on the temporal and geochemical evolution of the Selvagen Archipelago and neighbouring seamounts in the eastern North Atlantic. Journal of Volcanology and Geothermal Research 111, 55–87.
Geldmacher, J., Hoernle, K., Bogaard, P.V.D., Duggen, S., Werner, R., 2005. New $^{40}Ar/^{39}Ar$ age and geochemical data from seamounts in the Canary and Madeira volcanic provinces: Support for the mantle plume hypothesis. Earth and Planetary Science Letters 237, 85–101.
Guillou, H., Carracedo, J.C., Paris, R., Pérez Torrado, F.J., 2004. K/Ar ages and magnetic stratigraphy of the Miocene–Pliocene shield volcanoes of Tenerife, Canary Islands: implications for the early evolution of Tenerife and the Canarian hotspot age progression. Earth and Planetary Science Letters 222, 599–614.
Gurenko, A.A., Chaussidon, M., Schmincke, H.-U., 2001. Magma ascent and contamination beneath one intraplate volcano: evidence from S and O isotopes in glass inclusions and their host clinopyroxenes from Miocene basaltic hyaloclastites southwest of Gran Canaria (Canary Islands). Geochimica et Cosmochimica Acta 65, 4359–4374.
Gurenko, A.A., Hoernle, K.A., Hauff, F., Schmincke, H.-U., Han, D., Miura, Y.N., Kaneoka, I., 2006. Major, trace element and Nd–Sr–Pb–O–He–Ar isotope signatures of shield stage lavas from the central and western Canary Islands: Insights into mantle and crustal processes. Chemical Geology 233, 75–112.
Gurenko, A.A., Sobolev, A.V., Hoernlae, K.A., Hauff, F., Schmincke, H.-U., 2009. Enriched, HIMU-type peridotite and depleted recycled pyroxenite in the Canary plume: a mixed-up mantle. Earth and Planetary Science Letters 277, 514–524.
Gurenko, A.A., Hoernle, K.A., Sobolev, A.V., Hauff, F., Schmincke, H.-U., 2010. Source components of the Gran Canaria (Canary Islands) shield stage magmas: evidence from olivine composition and Sr–Nd–Pb isotopes. Contributions to Mineralogy and Petrology 159, 689–702.
Hamilton, A., Nelson, B., Carracedo, J., 2005. Evidence for shallow-level assimilation of the submarine volcanic complex underlying the NW rift zone of Tenerife, Canary Islands. American Geophysical Union, Fall Meeting 2005, abstract #V13E-0603.
Hanan, B.B., Graham, D.W., 1996. Lead and helium isotope evidence from oceanic basalts for a common deep source of mantle plumes. Science 272, 991–995.
Hansteen, T.H., Troll, V.R., 2003. Oxygen isotope composition of xenoliths from the oceanic crust and volcanic edifice beneath Gran Canaria (Canary Islands): consequences for crustal contamination of ascending magmas. Chemical Geology 193, 181–193.
Hansteen, T.H., Klügel, A., Schmincke, H.-U., 1998. Multi-stage magma ascent beneath the Canary Islands: evidence from fluid inclusions. Contributions to Mineralogy and Petrology 132, 48–64.
Harmon, R.S., Hoefs, J., 1995. Oxygen isotope heterogeneity of the mantle deduced from global ^{18}O systematics of basalts from different geotectonic settings. Contributions to Mineralogy and Petrology 120, 95–114.
Harris, C., Vogeli, J., 2010. Oxygen isotope composition of garnet in the peninsula granite, Cape granite suite, South Africa: constraints on melting and emplacement mechanisms. South African Journal of Geology 113 (4), 385–396.
Harris, C., Smith, H.S., le Roex, A.P., 2000. Oxygen isotope composition of phenocrysts from Tristan da Cunha and Gough Island lavas: variation with fractional crystallization and evidence for assimilation. Contributions to Mineralogy and Petrology 138, 164–175.
Hart, S.R., 1984. A large scale isotope anomaly in the Southern Hemisphere mantle. Nature 309, 753–757.
Hoernle, K., 1998. Geochemistry of Jurassic ocean crust beneath Gran Canaria (Canary Islands): implications for crustal recycling and assimilation. Journal of Petrology 39, 859–880.
Hoernle, K., Schmincke, H.-U., 1993. The role of partial melting in the 15-Ma geochemical evolution of Gran Canaria: a blob model for the Canary hotspot. Journal of Petrology 34, 599–626.
Hoernle, K., Tilton, G., Schmincke, H.-U., 1991. Sr–Nd–Pb isotopic evolution of Gran Canaria: evidence for shallow enriched mantle beneath the Canary Islands. Earth and Planetary Science Letters 106, 44–63.
Hoernle, K., Zhang, Y.-S., Graham, D., 1995. Seismic and geochemical evidence for large-scale mantle upwelling beneath the eastern Atlantic and western and central Europe. Nature 374, 34–39.
Hoffman, A., 1997. Mantle geochemistry: the message from oceanic volcanism. Nature 385, 219–229.
Irvine, T.N., Baragar, W.R.A., 1971. A guide to the chemical classification of the common volcanic rocks. Canadian Journal of Earth Sciences 8, 523–548.
Ito, E., White, W.M., Göpel, C., 1987. The O, Sr, Nd and Pb isotope geochemistry of MORB. Chemical Geology 62, 157–176.
Ito, G., Shen, Y., Hirth, G., Wolfe, C.J., 1999. Mantle flow, melting and dehydration of the Iceland mantle plume. Earth and Planetary Science Letters 165, 81–96.
Iwamori, H., McKenzie, D., Takahashi, E., 1995. Melt generation and isentropic mantle upwelling. Earth and Planetary Science Letters 134, 253–266.
Jochum, K.P., Verma, S.P., 1996. Extreme enrichment of Sb, Tl and other trace elements in altered MORB. Chemical Geology 130, 289–299.
Kent, A.J.R., Norman, M.D., Hutcheon, I.D., Stolper, E.M., 1999. Assimilation of seawater-derived components in an oceanic volcano: evidence from matrix glasses and glass inclusions from Loihi Seamount, Hawaii. Chemical Geology 156, 299–319.

Klügel, A., Hoernle, K.A., Schmincke, H.-U., White, J.D.L., 2000. The chemically zoned 1949 eruption on La Palma (Canary Islands): petrologic evolution and magma supply dynamics of a rift zone eruption. Journal of Geophysical Research 105, 5997–6016.
Le Maitre, R.W., Bateman, P., Dudek, A., Keller, J., Lameyre, J., Le Bas, M.J., Sabine, P.A., Schmid, R., Sorensen, H., Streckeisen, A., Woolley, A.R., Zanettin, B., 1989. A Classification of Igneous Rocks and Glossary of Terms. Blackwell, Oxford.
LeBas, M.J., Rex, D.C., Stillman, C.J., 1986. The early magmatic chronology of Fuerteventura, Canary Islands. Geological Magazine 123, 287–298.
Legendre, C., Maury, R.C., Caroff, M., Guillou, H., Cotton, J., Chauvel, C., Bollinger, C., Hémond, C., Guille, G., Blais, S., Rossi, P., Savanier, D., 2005. Origin of exceptionally abundant phonolites on Ua Pou Island (Marquesas, French Polynesia): partial melting of basanites followed by crustal contamination. Journal of Petrology 46, 1925–1962.
Longpré, M.-A., Troll, V.R., Walter, T.R., Hansteen, T.H., 2009. Volcanic and geochemical evolution of the Teno massif, Tenerife, Canary Islands: some repercussions of giant landslides on ocean island magmatism. Geochemistry, Geophysics, Geosystems 10 (Q12017, 31 pp.).
Luais, B., Telouk, P., Albarède, F., 1997. Precise and accurate neodymium isotopic measurements by plasma-source mass spectrometry. Geochimica et Cosmochimica Acta 61, 4847–4854.
Manconi, A., Longpré, M.-A., Walter, T.R., Troll, V.R., Hansteen, T.H., 2009. The effects of flank collapses on volcano plumbing systems. Geology 37, 1099–1102.
Marcantonio, F., Zindler, A., Elliott, T., Staudigel, H., 1995. Os isotope systematics of La Palma, Canary Islands: evidence for recycled crust in the mantle source of HIMU ocean islands. Earth and Planetary Science Letters 133, 197–410.
Martí, J., Hurlimann, M., Ablay, G.J., Gudmundsson, A., 1997. Vertical and lateral collapses on Tenerife (Canary Islands) and other volcanic ocean islands. Geology 25, 879–882.
Mattey, D., Lowry, D., Macpherson, C., 1994. Oxygen isotope composition of mantle peridotite. Earth and Planetary Science Letters 128, 231–241.
McDougall, I., Schmincke, H.U., 1976. Geochronology of Gran Canaria, Canary Islands: age of shield building volcanism and other magmatic phases. Bulletin of Volcanology 40, 1–21.
Montelli, R., Nolet, G., Dahlen, F.A., Masters, G., Engdahl, E.R., Hung, S.-H., 2004. Finite-frequency tomography reveals a variety of plumes in the mantle. Science 303, 338–343.
Morgan, W.J., 1983. Hotspot tracks and the early rifting of the Atlantic. Tectonophysics 94, 123–139.
Neumann, E.-R., Wulff-Pedersen, E., Simonsen, S.L., Pearson, N.J., Martí, J., Mitjavila, J., 1999. Evidence for fractional crystallization of periodically refilled magma chambers in Tenerife, Canary Islands. Journal of Petrology 40, 1089–1123.
O'Hara, M.J., 1998. Volcanic plumbing and the space problem. Thermal and geochemical consequences of large-scale assimilation in ocean island development. Journal of Petrology 39, 1077–1089.
Palacz, Z.A., Wolff, J.A., 1989. Strontium, neodymium and lead isotope characteristics of the Granadilla Pumice, Tenerife: a study of the causes of strontium isotope disequilibrium in felsic pyroclastic deposits. In: Saunders, A.D., Norry, M.J. (Eds.), Magmatism in the Ocean BasinsGeological Society Special Publication 42, 147–159.
Peccerillo, A., Dallai, L., Luce Frezzotti, M., Kempton, P.D., 2004. Sr–Nd–Pb–O isotopic evidence for decreasing crustal contamination with ongoing magma evolution at Alicudi volcano (Aeolian arc, Italy): implications for style of magma-crust interaction and for mantle source compositions. Lithos 78, 217–233.
Peucker-Ehrenbrink, B., Hofmann, A.W., Hart, S.R., 1994. Hydrothermal lead transfer from mantle to continental crust: the role of metalliferous sediments. Earth and Planetary Science Letters 125, 129–142.
Pin, C., Briot, D., Bassin, C., Poitrasson, F., 1994. Concomitant separation of strontium and samarium-neodymium for isotopic analysis in silicate samples, based on specific extraction chromatography. Analytica Chimica Acta 298, 209–217.
Raczek, I., Peter Jochum, K., Hofmann, A.W., 2003. Neodymium and strontium isotope data for USGS reference materials BCR-1, BCR-2, BHVO-1, BHVO-2, AGV-1, AGV-2, GSP-1, GSP-2 and eight MPI-DING reference glasses. Geostandards Newsletter 27, 173–179.
Roeser, H.A., 1982. Magnetic anomalies in the magnetic quiet zone off Morocco. In: Rad, U., Hinz, K., Sarnthein, M., Seibold, E. (Eds.), Geology of the Northwest African Continental Margin. Springer, Berlin, pp. 61–68.
Savin, S.M., Epstein, S., 1969. The oxygen and hydrogen isotope geochemistry of ocean sediments and shales. Geochimica et Cosmochimica Acta 34, 43–63.
Sheppard, S.M.F., Harris, C., 1985. Hydrogen and oxygen isotope geochemistry of Ascension Island lavas and granites: variation with crystal fractionation and interaction with seawater. Contributions to Mineralogy and Petrology 91, 74–81.
Simonsen, S.L., Neumann, E.-R., Seim, K., 2000. Sr–Nd–Pb isotope and trace-element geochemistry evidence for a young HIMU source and assimilation at Tenerife (Canary Island). Journal of Volcanology and Geothermal Research 103, 299–312.
Smith, H.J., Spivak, A.J., Staudigel, H., Hart, S.R., 1995. The boron isotopic composition of altered oceanic crust. Chemical Geology 126, 119–135.
Staudigel, H., Davies, G.R., Hart, S.R., Marchant, K.M., Smith, B.M., 1995. Large scale isotopic Sr, Nd and O isotopic anatomy of altered oceanic crust: DSDP/ODP sites 417/418. Earth and Planetary Science Letters 130, 169–185.
Stillman, C.J., Fúster, J.M., Bennell-Baker, M.J., Muñoz, M., Smewing, J.D., Sagredo, J., 1975. Basal complex of Fuerteventura (Canary Islands) is an oceanic intrusive complex with rift-system affinities. Nature 257, 469–471.
Stroncik, N.A., Klügel, A., Hansteen, T.H., 2009. The magmatic plumbing system beneath El Hierro (Canary Islands): constraints from phenocrysts and naturally quenched basaltic glasses in submarine rocks. Contributions to Mineralogy and Petrology 157, 593–607.
Sun, S.-S., McDonough, W.F., 1989. Chemical and isotopic systematics of oceanic basalts: implications for mantle composition and processes. In: Saunders, A.D., Norry, M.J. (Eds.), Magmatism in the Ocean Basins. : Special Publications, 42. Geological Society, London, pp. 313–345.
Taylor Jr., H.P., 1968. The oxygen isotope geochemistry of igneous rocks. Contributions to Mineralogy and Petrology 19, 1–71.
Taylor Jr., H.P., Sheppard, S.M.F., 1986. Igneous rocks: I. Processes of isotopic fractionation and isotope systematics. In: Valley, J.W., Taylor Jr., H.P., O'Neil, J.R. (Eds.), Stable isotopes in high temperature geological processesReviews in Mineralogy 16, 227–271.
Thirlwall, M.F., 1997. Pb isotopic evidence for OIB derivation from young HIMU mantle. Chemical Geology 139, 51–74.
Thirlwall, M.F., 2002. Multicollector ICP-MS analysis of Pb isotopes using a ^{207}Pb–^{204}Pb double spike demonstrates up to 400 ppm/amu systematic errors in Tl-normalization. Chemical Geology 184, 255–279.
Thirlwall, M.F., Jenkins, C., Vroon, P.Z., Mattey, D.P., 1997. Crustal interaction during construction of ocean islands: Pb–Sr–Nd–O isotope geochemistry of the shield basalts of Gran Canaria, Canary Islands. Chemical Geology 135, 233–262.
Thirlwall, M.F., Singer, B.S., Marriner, G.F., 2000. ^{39}Ar–^{40}Ar ages and geochemistry of the basaltic shield stage of Tenerife, Canary Islands, Spain. Journal of Volcanology and Geothermal Research 103, 247–297.
Troll, V.R., 2001. Evolution of large peralkaline silicic magma chambers and associated caldera systems: a case study from Gran Canaria, Canary Islands. Ph. D. thesis, Christian-Albrechts-Universität zu Kiel, p. 1–143.
Troll, V.R., Schmincke, H.-U., 2002. Alkali-feldspar in compositionally zoned peralkaline rhyolite/trachyte ignimbrite "A", Gran Canaria: implications for magma mixing and crustal recycling. Journal of Petrology 43, 243–270.
Troll, V.R., Klügel, A., Longpré, M.-A., Burchardt, S., Deegan, F.M., Carracedo, J.C., Wiesmaier, S., Kueppers, U., Dahren, B., Blythe, L.S., Hansteen, T.H., Freda, C., Budd, D.A., Jolis, E.M., Jonsson, E., Meade, F.C., Berg, S.E., Mancini, L., Polacci, M., Pedroza, K., 2012. Floating stones off El Hierro, Canary Islands: xenoliths of pre-island sedimentary origin in the early products of the October 2011 eruption. Solid Earth 3, 97–110.
Vennemann, T.W., Smith, H.S., 1990. The rate and temperature of reaction of ClF_3 with silicate minerals, and their relevance to oxygen isotope analysis. Chemical Geology (Isotope Geoscience Section) 86, 83–88.
Walter, T.R., Schmincke, H.-U., 2002. Rifting, recurrent landsliding and Miocene structural reorganization in NW-Tenerife (Canary Islands). International Journal of Earth Sciences 91, 615–628.
Walter, T.R., Troll, V.R., 2003. Experiments on rift zone formation in unstable volcanic edifices. Journal of Volcanology and Geothermal Research 127, 107–120.
Walter, T.R., Troll, V.R., Cailleau, B., Belousov, A., Schmincke, H.-U., Amelung, F., Van Den Bogaard, P., 2005. Rift zone reorganization through flank instability in ocean island volcanoes: an example from Tenerife, Canary Islands. Bulletin of Volcanology 67, 281–291.
Wang, Z., Eiler, J.M., 2008. Insights into the origin of low-$\delta^{18}O$ basaltic magmas in Hawaii revealed from in situ measurements of oxygen isotope compositions of olivines. Earth and Planetary Science Letters 269, 377–387.
Watts, A.B., Masson, D.G., 1995. A giant landslide on the north flank of Tenerife, Canary Islands. Journal of Geophysical Research 100, 24487–24498.
Weis, D., Kieffer, B., Maerschalk, C., Barling, J., de Jong, J., Williams, G.A., Hanano, D., Pretorius, W., Mattielli, N., Scoates, J.S., Goolaerts, A., Friedman, R.M., Mahoney, J.B., 2006. High-precision isotopic characterization of USGS reference materials by TIMS and MC-ICP-MS. Geochemistry, Geophysics, Geosystems 7 (Q08006, 30 pp.).
Widom, E., Hoernle, K.A., Shirey, S.B., Schmincke, H.-U., 1999. Os isotope systematics in the Canary Islands and Madeira: lithospheric contamination and mantle plume signatures. Journal of Petrology 40, 279–296.
Wiesmaier, S., 2010. Magmatic differentiation and bimodality in oceanic island settings – implications for the petrogenesis of magma in Tenerife, Spain. PhD thesis. University of Dublin, Trinity College.
Wiesmaier, S., Deegan, F.M., Troll, V.R., Carracedo, J.C., Chadwick, J.P., Chew, D., 2011. Magma mixing in the 100 AD Montaña Reventada composite eruption, Tenerife, Canary Islands: interaction between rift zone and central volcano plumbing systems. Contributions to Mineralogy and Petrology 162, 651–669.
Wiesmaier, S., Troll, V.R., Carracedo, J.C., Ellam, R.M., Bindeman, I.N., Wolff, J.A., 2012. Bimodality of lavas in the Teide–Pico Viejo succession in Tenerife — the role of crustal melting in the origin of recent phonolites. Journal of Petrology http://dx.doi.org/10.1093/petrology/egs056.
Wolff, J.A., Palacz, Z.A., 1989. Lead isotope and trace element variation in Tenerife pumices - evidence for recycling within an ocean island volcano. Min. Mag. 53, 519–525.
Wolff, J.A., Grandy, J.S., Larson, P.B., 2000. Interaction of mantle-derived magma with island crust? Trace element and oxygen isotope data from the Diego Hernandez Formation, Las Cañadas, Tenerife. Journal of Volcanology and Geothermal Research 130, 343–366.
Zindler, A., Hart, S., 1986. Chemical geodynamics. Annual Review of Earth and Planetary Science Letters 14, 493–571.